High organic inputs explain shallow and deep SOC storage in a long-term agroforestry system – Combining experimental and modeling approaches.

Rémi Cardinael[a,b,c,d*], Bertrand Guenet[e], Tiphaine Chevallier[a], Christian Dupraz[f], Thomas Cozzi[b], Claire Chenu[b]

[a] Eco&Sols, IRD, CIRAD, INRA, Montpellier SupAgro, Univ Montpellier, Montpellier, France

[b] AgroParisTech, UMR Ecosys, Avenue Lucien Brétignières, 78850 Thiverval-Grignon, France

[c] CIRAD, UPR AIDA, F-34398 Montpellier, France (present address)

[d] AIDA, Univ Montpellier, CIRAD, Montpellier, France

[e] Laboratoire des Sciences du Climat et de l'Environnement, UMR CEA-CNRS-UVSQ, CE L'Orme des Merisiers, 91191 Gif-Sur-Yvette, France

[f] System, INRA, CIRAD, Montpellier SupAgro, Univ Montpellier, Montpellier, France

* Corresponding author. Tel.: +33 04.67.61.53.08. E-mail address: remi.cardinael@cirad.fr

Keywords: priming effect, deep roots, deep soil organic carbon, spatial heterogeneity, silvoarable system, crop yield, SOC modeling

Abstract

Agroforestry is an increasingly popular farming system enabling agricultural diversification and providing several ecosystem services. In agroforestry systems, soil organic carbon (SOC) stocks are generally increased, but it is difficult to disentangle the different factors responsible for this storage. Organic carbon (OC) inputs to the soil may be larger, but SOC decomposition rates may be modified owing to microclimate, physical protection, or priming effect from roots, especially at depth. We used an 18-year-old silvoarable system associating hybrid walnut trees

(*Juglans regia* × *nigra*) and durum wheat (*Triticum turgidum* L. subsp. *durum*), and an adjacent agricultural control plot to quantify all OC inputs to the soil - leaf litter, tree fine root senescence, crop residues, and tree row herbaceous vegetation -, and measure SOC stocks down 2 m depth at varying distances from the trees. We then proposed a model that simulates SOC dynamics in agroforestry accounting for both the whole soil profile and the lateral spatial heterogeneity. The model was calibrated to the control plot only.

Measured OC inputs to soil were increased by about 40% (+ 1.11 t C ha^{-1} yr^{-1}) down to 2 m depth in the agroforestry plot compared to the control, resulting in an additional SOC stock of 6.3 t C ha^{-1} down to 1 m depth. The model was strongly validated, describing properly the measured SOC stocks and distribution with depth in agroforestry tree rows and alleys. It showed that the increased inputs of fresh biomass to soil explained the observed additional SOC storage in the agroforestry plot. Moreover, only a priming effect variant of the model was able to capture the depth distribution of SOC stocks. This result questions the potential of soils to store large amounts of carbon, especially at depth. Deep-rooted trees modify OC inputs to soil, a process that deserves further studies given its potential effects on SOC dynamics.

1 Introduction

Agroforestry systems are complex agroecosystems combining trees and crops or pastures within the same field (Nair, 1993, 1985; Somarriba, 1992). More precisely, silvoarable systems associate parallel tree rows with annual crops. Some studies showed that these systems could be very productive, with a land equivalent ratio (Mead and Willey, 1980) reaching up to 1.3 (Graves et al., 2007). Silvoarable systems may therefore produce up to 30% more marketable biomass on the same area of land compared to crops and trees grown separately. This performance can be explained by a better use of water, nutrients and light by the agroecosystem throughout the year. Trees grown in silvoarable systems usually grow faster than the same trees

51 grown in forest ecosystems, because of their lower density, and because they also benefit from
52 the crop fertilization (Balandier and Dupraz, 1999; Chaudhry et al., 2003; Chifflot et al., 2006).
53 In temperate regions, farmers usually grow one crop per year, and this association of trees can
54 extend the growing period at the field scale, especially when winter crops are intercropped with
55 trees having a late bud break (Burgess et al., 2004). However, after several years, a decrease of
56 crop yield can be observed in mature and highly dense plantations, especially close to the trees,
57 due to competition between crops and trees for light, water, and nutrients (Burgess et al., 2004;
58 Dufour et al., 2013; Yin and He, 1997).
59 Part of the additional biomass produced in agroforestry is used for economical purposes, such
60 as timber or fruit production. Leaves, tree fine roots, pruning residues and the herbaceous
61 vegetation growing in the tree rows will usually return to the soil, contributing to a higher input
62 of organic carbon (OC) to the soil compared to an agricultural field (Peichl et al., 2006).
63 In such systems, the observed soil organic carbon (SOC) stocks are also generally higher
64 compared to a cropland (Albrecht and Kandji, 2003; Kim et al., 2016; Lorenz and Lal, 2014).
65 Cardinael *et al.*, (2017) measured a mean SOC stock accumulation rate of 0.24 (0.09-0.46) t C
66 ha^{-1} yr^{-1} at 0-30 cm depth in several silvoarable systems compared to agricultural plots in
67 France. Higher SOC stocks were also found in Canadian agroforestry systems, but measured
68 only to 20 cm depth (Bambrick et al., 2010; Oelbermann et al., 2004; Peichl et al., 2006).
69 To our knowledge, we are still not able to disentangle the factors responsible for such a higher
70 SOC storage. This SOC storage might be due to higher OC inputs but it could also be favored
71 by a modification of the SOC decomposition owing to a change in SOC physical protection
72 (Haile et al., 2010), and/or in soil temperature and moisture.
73 The introduction of trees in an agricultural field modifies the amount, but also the distribution
74 of fresh organic carbon (FOC) input to the soil, both vertically and horizontally (Bambrick et
75 al., 2010; Howlett et al., 2011; Peichl et al., 2006). FOC inputs from the trees decrease with

increasing distance from the trunk and with soil depth (Moreno et al., 2005). On the contrary, crop yield usually increases with increasing distance from the trees (Dufour et al., 2013; Li et al., 2008). Therefore, the proportions of FOC coming from both the crop residues and the trees change with distance from the trees, soil depth, and time.

Tree fine roots (diameter ≤ 2 mm) are the most active part of root systems (Eissenstat and Yanai, 1997) and play a major role in carbon cycling. In silvoarable systems, tree fine root distribution within the soil profile is strongly modified due to the competition with the crop, inducing a deeper rooting compared to trees grown in forest ecosystems (Cardinael et al., 2015a; Mulia and Dupraz, 2006). Deep soil layers may therefore receive significant OC inputs from fine root mortality and exudates. Root carbon has a higher mean residence time in the soil compared to shoot carbon (Kätterer et al., 2011; Rasse et al., 2006), presumably because root residues are preferentially stabilized within microaggregates or adsorbed to clay particles. Moreover, temperature and moisture conditions are more buffered in the subsoil than in the topsoil. The microbial biomass is also smaller at depth (Eilers et al., 2012; Fierer et al., 2003), and the spatial segregation with organic matter is larger (Salomé et al., 2010) resulting in lower decomposition rates. Deep root carbon input in the soil could therefore contribute to a SOC storage with high mean residence times. However, some studies showed that adding FOC – a source of energy for microorganisms - to the subsoil enhanced decomposition of stabilized carbon, a process called « priming effect » (Fontaine et al., 2007). The priming effect is stronger when induced by labile molecules like root exudates than by root litter coming from the decomposition of dead roots (Shahzad et al., 2015). Therefore, the net effect of deep roots on SOC stocks has to be assessed, especially in silvoarable systems.

Models are crucial as they allow virtual experiments to best design and understand complex processes in these systems (Luedeling et al., 2016). Several models have been developed to simulate interactions for light, water and nutrients between trees and crops (Charbonnier et al.,

2013; Duursma and Medlyn, 2012; van Noordwijk and Lusiana, 1999; Talbot, 2011) or to predict tree growth and crop yield in agroforestry systems (Graves et al., 2010; van der Werf et al., 2007). However, none of these models are designed to simulate SOC dynamics in agroforestry systems and they are therefore not useful to estimate SOC storage. Oelbermann & Voroney (2011) evaluated the ability of the CENTURY model (Parton et al., 1987) to predict SOC stocks in tropical and temperate agroforestry systems, but with a single-layer modeling approach (0-20 cm). The approach of modeling a single topsoil layer assumes that deep SOC does not play an active role in carbon cycling, while it was shown that deep soil layers contain important amounts of SOC (Jobbagy and Jackson, 2000), and that part of this deep SOC could cycle on decadal timescales due to root inputs or to dissolved organic carbon transport (Baisden and Parfitt, 2007; Koarashi et al., 2012). The need to take into account deep soil layers when modeling SOC dynamics is now well recognized in the scientific community (Baisden et al., 2002; Elzein and Balesdent, 1995), and several models have been proposed (Braakhekke et al., 2011; Guenet et al., 2013; Koven et al., 2013; Taghizadeh-Toosi et al., 2014; Ahrens et al., 2015). Using vertically discretized soils is particularly important when modeling the impact of agroforestry systems on SOC stocks, but to our knowledge, vertically spatialized SOC models have not yet been tested for these systems.

The aims of this study were then twofold: (i) to propose a model of soil C dynamics in agroforestry systems able to account for both vertical and lateral spatial heterogeneities and (ii) to test whether variations of fresh organic carbon (FOC) input could explain increased SOC stocks both using experimental data and model runs.

For this, we first compiled data on FOC inputs to the soil obtained in a 18-year-old agroforestry plot and in an agricultural control plot in southern France, in which SOC stocks have been recently quantified to 2 m depth (Cardinael et al., 2015b). FOC inputs comprised tree fine roots,

126 tree leaf litter, aboveground and belowground biomass of the crop and of the herbaceous
127 vegetation in the tree rows. We compiled recently published data for FOC inputs (Cardinael et
128 al., 2015a; Germon et al., 2016), and measured the others (Table 1).
129
130 We then modified a two pools model proposed by Guenet *et al.*, (2013), to create a spatialized
131 model over depth and distance from the tree, the CARBOSAF model (soil organic CARBOn
132 dynamics in Silvoarable AgroForestry systems). Based on data acquired since the tree planting
133 in 1995 (crop yield, tree growth), and on FOC inputs, we modeled SOC dynamics to 2 m depth
134 in both the silvoarable and agricultural control plot. We evaluated the model against measured
135 SOC stocks along the profile and used this opportunity to test the importance of priming effect
136 (*PE*) for deep soil C dynamics in a silvoarable system. The performance of the two pools model
137 including *PE* was also compared with a model version including three OC pools.
138
139 **2 Materials and methods**
140 **2.1 Study site**
141 The experimental site is located at the Restinclières farm Estate in Prades-le-Lez, 15 km North
142 of Montpellier, France (longitude 04°01' E, latitude 43°43' N, elevation 54 m a.s.l.). The
143 climate is sub-humid Mediterranean with an average temperature of 15.4°C and an average
144 annual rainfall of 973 mm (years 1995–2013). The soil is a silty and carbonated (pH = 8.2) deep
145 alluvial Fluvisol (IUSS Working Group WRB, 2007). In February 1995, a 4.6 hectare
146 silvoarable agroforestry plot was established with the planting of hybrid walnut trees (*Juglans*
147 *regia* × *nigra* cv. NG23) at a density of 192 trees ha^{-1} but later thinned to 110 trees ha^{-1}. Trees
148 were planted at 13 m × 4 m spacing, and tree rows are East–West oriented. The cultivated alleys
149 are 11 m wide. The remaining part of the plot (1.4 ha) was kept as an agricultural control plot.
150 Since the tree planting, the agroforestry alleys and the control plot were managed in the same

151 way. The associated crop is most of the time durum wheat (*Triticum turgidum* L. subsp. *durum*),
152 except in 1998, 2001 and 2006, when rapeseed (*Brassica napus* L.) was cultivated, and in 2010
153 and 2013, when pea (*Pisum sativum* L.) was cultivated. The soil is ploughed to a depth of 0.2
154 m before sowing, and the wheat crop is fertilized with an average of 120 kg N ha^{-1} yr^{-1}. Crop
155 residues (wheat straw) are also exported, but about 25% remain on the soil. Tree rows are
156 covered by spontaneous herbaceous vegetation. Two successive herbaceous vegetation types
157 occur during the year, one in summer and one in winter. The summer vegetation is mainly
158 composed of *Avena fatua* L., and is 1.5 m tall. In winter, the vegetation is a mix of *Achillea*
159 *millefolium* L., *Galium aparine* L., *Vicia* L., *Ornithogalum umbellatum* L. and *Avena fatua* L,
160 and is 0.2 m tall.
161
162 **Table 1.** Synthesis of the different field and laboratory data available or measured, and their
163 sources.

Description of the data	Source
Soil texture, bulk densities, SOC stocks	Cardinael *et al.*, (2015a)
Soil temperature and soil moisture	Measured
Tree growth (DBH)	Measured
Tree wood density	(Talbot, 2011)
Tree fine root biomass	Cardinael *et al.*, (2015b)
Tree fine root turnover	Germon *et al.*, (2016)
Crop yield and crop ABG biomass	Dufour *et al.*, (2013) and measured
Crop root biomass	Prieto *et al.*, (2015) and measured
Tree row herbaceous vegetation – ABG biomass	Measured
Tree row herbaceous vegetation – root biomass	Measured
Biomass carbon concentrations	Measured
Potential decomposition rate of roots	Prieto *et al.*, (2016a)
HSOC potential decomposition rate	Measured

164 DBH: Diameter at Breast Height; ABG: aboveground; OC: organic carbon; HSOC: humified
165 soil organic carbon.
166
167 **2.2 Organic carbon stocks**
168 **2.2.1 Soil organic carbon stocks**

SOC data have been published in Cardinael *et al.*, (2015b). Briefly, soil cores were sampled down to 2 m depth in May 2013, 100 in the agroforestry plot, and 93 in the agricultural control plot. SOC concentrations, soil bulk densities, SOC stocks, and soil texture were measured for ten soil layers (0.0-0.1, 0.1-0.3, 0.3-0.5, 0.5-0.7, 0.7-1.0, 1.0-1.2, 1.2-1.4, 1.4-1.6, 1.6-1.8, and 1.8-2.0 m). In the agroforestry plot, 40 soil cores were taken in the tree rows, while 60 were sampled in the alleys at varying distances from the trees. Soil organic carbon stocks were quantified on an equivalent soil mass basis (Ellert and Bettany, 1995).

2.2.2 Tree aboveground and stump carbon stocks

Three hybrid walnuts were chopped down in 2012. The trunk circumference was measured every meter up to the maximum height of the tree to estimate its volume. The trunk biomass was estimated by multiplying the trunk volume by the wood density that was measured at 616 kg m^{-3} during a previous work at the same site (Talbot, 2011). Then, branches were cut, the stump was uprooted, and they were weighted separately. Samples were brought to the laboratory to determine the moisture content, which enabled calculation of the branches and the stump dry mass.

2.3 Measurements of organic carbon inputs in the field

2.3.1 Carbon inputs from tree fine root mortality

The tree fine root (diameter $\leq$ 2 mm) biomass was quantified and coupled with an estimate of the tree fine root turnover in order to predict the carbon input to the soil from the tree fine root mortality. A detailed description of the methods used to estimate the tree fine root biomass can be found in Cardinael *et al.*, (2015a). In March 2012, a 5 (length) × 1.5 (width) × 4 m (depth) pit was open in the agroforestry plot, perpendicular to the tree row, at the North of the trees. The tree fine root distribution was mapped down 4 m depth, and the tree fine root biomass was

quantified in the tree row and in the alley. Only results concerning the first two meters of soil, among those obtained by Cardinael *et al.*, (2015a) will be used here.

In July 2012, sixteen minirhizotrons were installed in the agroforestry pit, at 0, 1, 2.5 and 4 m depth, and at two and five meters from the trees. The tree root growth and mortality was monitored during one year using a scanner (CI-600 Root Growth Monitoring System, CID, USA), and analyzed using the WinRHIZO Tron software (Régent, Canada). A detailed description of the methods and of results used to estimate the tree fine root turnover can be found in Germon *et al.*, (2016).

2.3.2 Tree litterfall

In 2009, the crowns of two walnut trees were packed with a net in order to collect the leaf biomass from September to January. The same was done in 2012 with three other walnut trees. The leaf litter was then dried, weighted and analyzed for C to quantify the leaf carbon input per tree.

2.3.3 Aboveground and belowground input from the crop

Since the tree planting in 1995, the crop yield was measured 14 times (in 1995, 2000, 2002, 2003, 2004, 2005, 2007, 2008, 2009, 2010, 2011, 2012, 2013, and 2014), while the wheat straw biomass and the total aboveground biomass were measured six times (in 2007, 2008, 2009, 2011, 2012, and 2014) in both the control and the agroforestry plot (Dufour et al., 2013), using sampling subplots of 1 m^2 each. In the control plot, five subplots have been sampled while in the agroforestry plot five transects have been sampled. Each transect was made of three subplots, 2 m North from the tree, 2 m South from the tree, and 6.5 m from the tree (middle of the alley). In March 2012, a 2 m deep pit was opened in the agricultural control plot (Prieto et al., 2015), and the root biomass was quantified to the maximum rooting depth (1.5 m). The

219 root:shoot ratio of durum wheat was measured in the control plot. We assumed that the crop
220 root biomass turns out once a year, after the crop harvest.
221
222 **2.3.4 Above and belowground input from the tree row herbaceous vegetation**
223 As two types of herbaceous vegetation grow in the tree rows during the year, samples were
224 taken in summer and winter. In late June 2014, twelve subplots of 1 m^2 each were positioned
225 in the tree rows, around 4 walnut trees. In January 2015, six subplots of 1 m^2 each were
226 positioned in the tree rows, around 2 walnut trees. The middle of each subplot was located at 1
227 m, 2 m and 3 m, respectively, from the selected walnut tree. All the aboveground vegetation
228 was collected in each square. In the middle of each subplot, root biomass was sampled with a
229 cylindrical soil corer (inner diameter of 8 cm). Soil was taken at three soil layers, 0.0-0.1, 0.1-
230 0.3 and 0.3-0.5 m. In the laboratory, soil was gently washed with water through a 2 mm mesh
231 sieve, and roots were collected. Roots from the herbaceous vegetation were easily separated
232 manually from walnut roots, as they were soft and yellow compared to walnuts roots that were
233 black. After being sorted out from the soil and cleaned, the root biomass was dried at 40°C and
234 measured.
235
236 **2.4 Carbon concentration measurements**
237 All organic carbon measurements were performed with a CHN elemental analyzer (Carlo Erba
238 NA 2000, Milan, Italy), after samples were oven-dried at 40°C for 48 hours (Table 2). Dry
239 biomasses (t DM ha^{-1}) of each organic matter inputs were multiplied by their respective organic
240 carbon concentrations (mg C g^{-1}) to calculate organic carbon stocks (t C ha^{-1}).
241
242 **Table 2.** Organic carbon concentrations and C:N ratio of the different types of biomass.

Type of biomass	Organic C concentration (mg C g^{-1})	C:N	Number of replicates

Walnut trunk	445.7 ± 1.0	159.1 ± 25.2	3
Walnut branches	428.6 ± 1.7	62.2 ± 11.7	3
Wheat straw	433.2 ± 0.7	55.5 ± 2.1	5
Wheat root	351.4 ± 19	24.8 ± 2.1	8
Walnut leaf	449.4 ± 3.7	49.1 ± 0.4	3
Walnut fine root	437.0 ± 3.3	28.6 ± 3.4	8
Summer vegetation (ABG)	448.4 ± 1.9	37.8 ± 2.2	5
Summer vegetation (roots)	314.5 ± 8.3	33.8 ± 1.7	6
Winter vegetation (ABG)	447.7 ± 5.3	11.2 ± 0.4	3
Winter vegetation (roots)	397.4 ± 5.0	24.7 ± 0.7	3

The organic matter called "vegetation" stands for the herbaceous vegetation that grows in the tree row. ABG: aboveground. Errors represent standard errors.

2.5 General description of the CARBOSAF model

2.5.1 Organic carbon decomposition

We adapted a model developed by Guenet et al. (2013) where total SOC is split in two pools, the FOC and the humified soil organic carbon (HSOC) for each soil layer (Fig. 1a). Input to the FOC pool comes from the plant litter and the distribution of this input within the profile is assumed to depend upon depth from the surface (z), distance from the tree (d), and time (t). Equations describing inputs to the FOC pool ($I_{t,z,d}$) at a given time, depth, and distance are fully explained in the Results.

The FOC mineralisation is assumed to be governed by first order kinetics, being proportional to the FOC pool, as given by:

$$dec\_FOC_{t,z,d} = -k_{FOC} \times FOC_{t,z,d} \times f_{clay,z} \times f_{moist,z} \times f_{temp,z} \qquad (1)$$

where $FOC_{t,z,d}$ is the FOC carbon pool (kg C m^{-2}) at a given time (t, in years), depth (z, in m) and distance (d, in m), and k_{FOC} is its decomposition rate. The potential decomposition rates of the different plant materials were assessed with a 16-week incubation experiment during a companion study at the site (Prieto et al., 2016). The decomposition rate k_{FOC} was weighted by the respective contribution of each type of plant litter as a function of the tree age, soil depth

and distance from the tree. The rate modifiers $f_{clay,z}$, $f_{moist,z}$ and $f_{temp,z}$ are functions depending respectively on the clay content, soil moisture and soil temperature at a given depth z, and range between 0 and 1.

The f_{clay} function originated from the CENTURY model (Parton et al., 1987):

$$f_{clay,z} = 1 - 0.75 \times Clay_z \qquad (2)$$

where $Clay_z$ is the clay fraction (ranging between 0 and 1) of the soil at a given depth z.

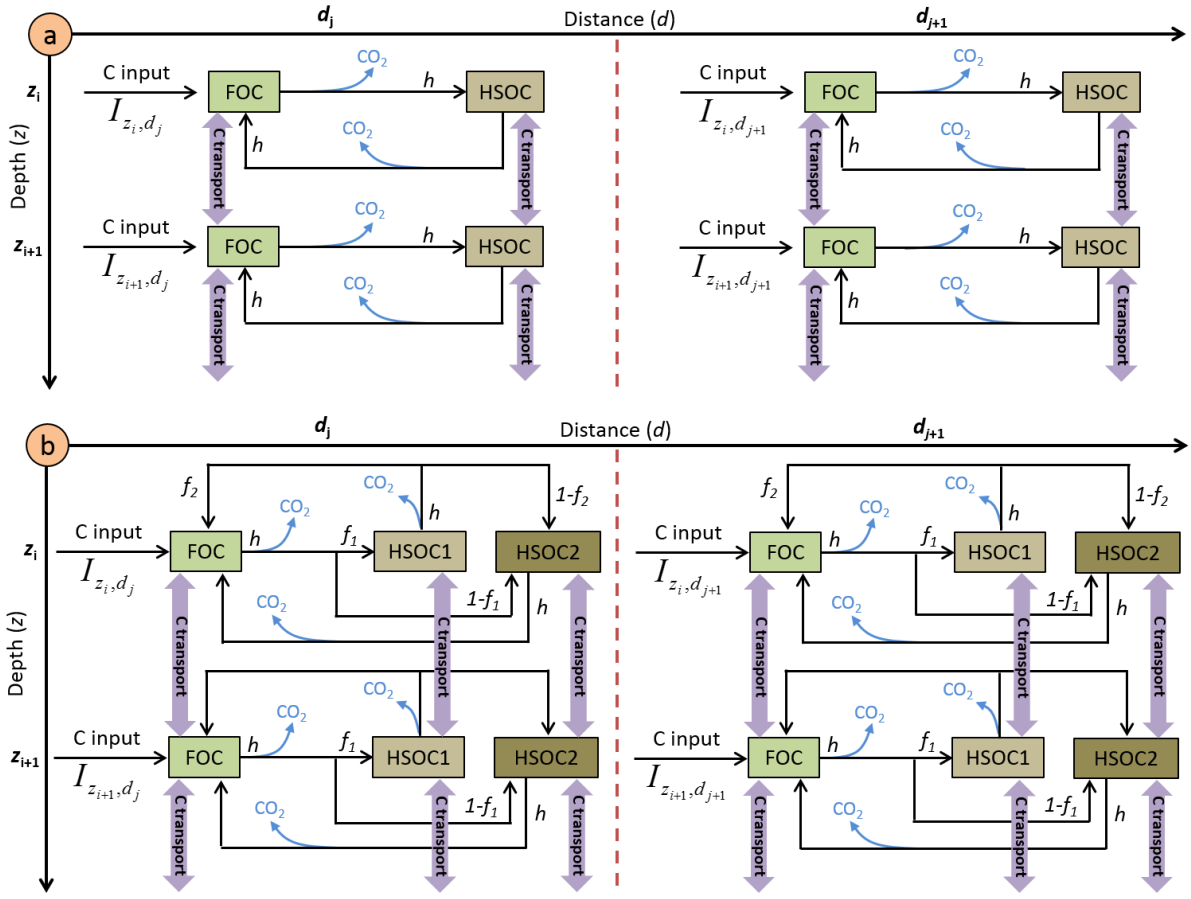

Fig. 1. Schematic representation of the pools and the fluxes of the (a) two pools model and (b) three pools model.

The $f_{moist,z}$ function originated from the meta-analysis of Moyano *et al.*, (2012) and is affected by soil properties (clay content, SOC content). Briefly, the authors fitted linear models on 310 soil incubations to describe the effect of soil moisture on decomposition. Then, they normalized such linear models between 0 and 1 to apply these functions to classical first order kinetics. All details are described in Moyano *et al.*, (2012). To save computing time, we calculated $f_{moist,z}$ only once using measured SOC stocks instead of using modelled SOC stocks and repeated the calculation at each time step.

The temperature sensitivity of the soil respiration is expressed as Q_{10}:

$$f_{temp,z} = Q_{10}^{\frac{temp_z - temp_{opt}}{10}} \quad (3)$$

with $temp_z$ being the soil temperature in K at each soil depth z and $temp_{opt}$ a parameter fixed to 304.15 K. The Q_{10} value was fixed to 2, a classical value used in models (Davidson and Janssens, 2006).

Once the FOC is decomposed, a fraction is humified (h) and another is respired as CO_2 ($1-h$) (Fig. 1a) following equations (4) and (5).

$$Humified\ FOC_{t,z,d} = h \times dec\_FOC_{t,z,d} \quad (4)$$

$$Respired\ FOC_{t,z,d} = (1-h) \times dec\_FOC_{t,z,d} \quad (5)$$

Two mathematical approaches are available in the model to describe the mineralisation of HSOC: a first order kinetics, as given by Eq. (6) or an approach developed by Wutzler & Reichstein, (2008) and by Guenet *et al.*, (2013) introducing the priming effect, i.e., the mineralisation of HSOC depends on FOC availability, and given by Eq. (7):

$$dec\_HSOC_{t,z,d} = -k_{HSOC,z} \times HSOC_{t,z,d} \times f_{moist,z} \times f_{temp,z} \quad (6)$$

$$dec\_HSOC_{t,z,d} = -k_{HSOC,z} \times HSOC_{t,z,d} \times (1 - e^{-PE \times FOC_{t,z,d}}) \times f_{moist,z} \times f_{temp,z} \quad (7)$$

where $HSOC_{t,z,d}$ is the humified SOC carbon pool at a given time (t, in years), depth (z, in m) and distance (d, in m), $k_{HSOC,z}$ is its decomposition rate (yr^{-1}) at a given depth z, and PE is the priming effect parameter. The parameters $f_{moist,z}$ and $f_{temp,z}$ are functions depending respectively on soil moisture and soil temperature at a given depth z, and affecting the decomposition rate of HSOC. They correspond to the moisture equation from Moyano *et al.*, (2012) and to Eq. (3), respectively. The decomposition rate $k_{HSOC,z}$ was an exponential law depending on soil depth (z) as shown by an incubation study (see paragraph *HSOC decomposition rate* further in the M&M):

$$k_{HSOC,z} = a \times e^{-b \times z} \quad (8)$$

The b parameter of this equation represented the ratio of labile C/stable C within the HSOC pool. The effect of clay on HSOC decomposition was implicitly taken into account in this equation as clay content increased with soil depth.

A fraction of decomposed HSOC returns to the FOC assuming that part of the HSOC decomposition products is as labile as FOC (h) and another is respired as CO_2 (Fig. 1a) in the two pools model.

Finally, we also developed an alternative version of the model with three pools by splitting the HSOC pools into two pools with different turnover rates, HSOC2 being more stabilized than HSOC1 (Fig. 1b). The non-respired decomposed FOC is split between HSOC1 and HSOC2 following a parameter f_1. The non-respired decomposed HSOC1 is split between HSOC2 and FOC following a parameter f_2 whereas non-respired decomposed HSOC2 is only redistributed into the FOC pools. The decomposition of HSOC1 and HSOC2 both follow the equation (8) but with different parameter values for a.

2.5.2 Carbon transport mechanisms

The transport of C between the different soil layers was represented by both advection and diffusion mechanisms (Elzein and Balesdent, 1995), which have been shown to usually describe well the C transport in soils (Bruun et al., 2007; Guenet et al., 2013). The advection represents the C transport due to the water infiltration in the soil, while the diffusion represents the C transport due to the fauna activity. The same transport coefficients were applied to the two C pools, FOC and HSOC.

The advection is defined by:

$$F_A = A \times C \qquad (9)$$

where F_A is the flux of *C* transported downwards by advection, and *A* is the advection rate (mm yr^{-1}).

The diffusion is represented by the Fick's law:

$$F_D = -D \times \frac{\partial^2 C}{\partial z^2} \qquad (10)$$

where F_D is the flux of C transported downwards by diffusion, $-D$ the diffusion coefficient (cm^2 yr^{-1}) and *C* the amount of carbon in the pool subject to transport (FOC or HSOC).

To represent the effect of soil tillage ($z \leq 0.2$ m), we added another diffusion term using the Fick's law but with a value of *D* several orders of magnitude higher to represent the mixing due to tillage. It must be noted that no tillage effect on the decomposition was represented here because of the large unknowns on these aspects (Dimassi et al., 2013; Virto et al., 2012).

In this model, the flux of *C* transported downwards by the advection and diffusion (F_{AD}) was represented as the sum of both mechanisms, following Elzein & Balesdent (1995):

$$F_{AD} = F_A + F_D \qquad (11)$$

The FOC and HSOC pools dynamics in the two pools model correspond to:

$$\frac{\partial FOC_{t,z,d}}{\partial t} = I_{t,z,d} + \frac{\partial F_{AD}}{\partial z} + h \times dec\_HSOC_{t,z,d} - dec\_FOC_{t,z,d} \qquad (12)$$

$$\frac{\partial HSOC_{t,z,d}}{\partial t} = \frac{\partial F_{AD}}{\partial z} + h \times dec\_FOC_{t,z,d} - dec\_HSOC_{t,z,d} \qquad (13)$$

Finally, the FOC, HSOC1 and HSOC2 pools dynamics in the three pools model correspond to:

$$\frac{\partial FOC_{t,z,d}}{\partial t} = I_{t,z,d} + \frac{\partial F_{AD}}{\partial z} + h \times f_2 \times dec\_HSOC1_{t,z,d} + h \times dec\_HSOC2_{t,z,d} - dec\_FOC_{t,z,d} \qquad (14)$$

$$\frac{\partial HSOC1}{\partial t\partial} = \frac{\partial F_{AD}}{\partial z} + h \times f_1 \times dec\_FOC_{t,z,d} - dec\_HSOC1_{t,z,d} \qquad (15)$$

$$\frac{\partial HSOC2}{\partial t} = \frac{\partial F_{AD}}{\partial z} + h \times (1 - f_1) \times dec\_FOC_{t,z,d} + h \times (1 - f_2) \times dec\_HSOC1_{t,z,d} - dec\_HSOC2_{t,z,d} \qquad (16)$$

2.5.3 Depth dependence of HSOC potential decomposition rates

The shape of the function (i.e. the *b* parameter) describing the HSOC potential decomposition rate (Eq. (8)) was determined by incubating soils from the control, the alley and the tree row, and from different soil layers (0.0-0.1, 0.1-0.3, 0.7-1.0 and 1.6-1.8 m). Soils were sieved at 5 mm, and incubated during 44 days at 20°C at a water potential of -0.03 MPa. Evolved CO_2 was measured using a micro-GC at 1, 3, 7, 14, 21, 28, 35, 44 days. The three first measurement dates corresponded to a pre-incubation period and were not included in the analysis. For a given depth, the cumulative mineralised SOC was expressed as a percentage of total SOC and was

plotted against the incubation time. The slopes represented the potential SOC mineralisation rate at a given soil depth and location. The potential SOC mineralisation rates were then plotted against soil depth (Fig. S1). We used the soil incubations to determine only the *b* parameter of the curve: with such short term incubations, the SOC decomposition rate over the soil profile is overestimated because the CO_2 measured during the incubations mainly originates from the labile C pool. The *a* parameter was optimized following the procedure described further.

2.6 Boundary conditions of the CARBOSAF model

2.6.1 Annual aggregates of soil temperature and soil moisture

In April 2013, eight soil temperature and moisture sensors (Campbell CS 616 and Campbell 107, respectively) were installed in the agroforestry plot at 0.3, 1.3, 2.8 and 4.0 m depth, and at 2 and 5 m from the trees. Soil temperature and moisture were measured for 11 months.

The mean annual soil temperature in the agroforestry plot was described by the following equation:

$$T = -0.89 \times z + 288.24 \qquad (R^2 = 0.99) \qquad (17)$$

where *T* is the soil temperature (K) and *z* is the soil depth (m).

The mean annual soil moisture was described with the following equation:

$$\theta = 0.05 \times z + 0.28 \qquad (R^2 = 0.99) \qquad (18)$$

where θ is the soil volumetric moisture (cm cm^{-3}) and *z* is the soil depth (m).

Due to a lack of data in the agricultural plot, we assumed that the soil temperature and the soil moisture were the same in the agroforestry tree rows, alleys and in the control plot, but we further performed a sensitivity analysis of the model on these two parameters.

2.6.2 Interpolation of tree growth

The tree growth has been measured in the field since the establishment of the experiment. We used the diameter at breast height (*DBH*) as a surrogate of the tree growth preferentially to the tree height as the field measurements were more accurate. Indeed, *DBH* is easier to measure than height, especially when trees are getting older. To describe the temporal dynamic of *DBH* since the tree planting, a linear equation was fitted on the data.

Tree growth measurements enabled us to fit the following equation that was used in the model:

$$DBH_t \begin{cases} 0.01, & t \leq 3 \\ 0.0157 \times t - 0.0391 \ (R^2 = 0.997) & 3 < t \leq 20 \end{cases} \quad (19)$$

where DBH_t is the diameter at breast height (m) and t represents the time since tree planting (years).

2.6.3 Change of tree litterfall over time

For the five walnut trees where the leaf biomass was quantified, *DBH* was also measured. The ratio between the leaf biomass and *DBH* was then calculated for the five replicates. Total leaf biomass was 8.96 ± 1.45 kg DM tree^{-1} and the carbon concentration of walnut leaves was 449.4 ± 3.7 mg C g^{-1} (Table 2). With a density of 110 trees ha^{-1}, leaf litterfall was estimated at 0.73 ± 0.06 t C ha^{-1} in 2012 and at the plot scale. The ratio between leaf biomass and *DBH* was 0.0277 ± 0.0024 t C tree^{-1} m^{-1} or 3.05 t C ha^{-1} m^{-1}. The following linear relationship was therefore used in the model to describe leaf litter C input with the tree growth:

$$L_t = 3.05 \times DBH_t \quad (20)$$

where L_t is the leaf litter input (t C ha^{-1}) at the year t, and DBH_t the diameter at breast height (m) the year t.

2.6.4 Tree fine root C input from mortality

In 2012, the measured tree fine root biomass was higher in the tree row than in the alley (Table S1). From 0 to 1 m distance from the tree (in the tree row), the tree fine root biomass was homogeneous and was 1.01 t C ha^{-1} down 2 m depth.

In 2012 and in the alley, the tree fine root biomass (*TFRB*) decreased with increasing distance from the tree and was represented by an exponential function:

$$TFRB = \begin{cases} 1.01, & 0 \le d \le 1 \\ 1.29 \times e^{-0.28 \times d} \quad (R^2 = 0.90), & 1 < d \le 6.5 \end{cases} \qquad (21)$$

where *TFRB* represents tree fine root biomass down 2 m depth (t C ha^{-1}), and *d* the distance from the tree (m).

We considered a linear increase of *TFRB* with increasing *DBH*, and a linear regression was performed between *TFRB* in 2012 and *TFRB* in 1996, the first year after planting (biomass considered as negligible). The following linear relationship was used to simulate *TFRB* as a function of tree growth:

$$TFRB_{t,d} = \begin{cases} 3.69 \times DBH_t, & 0 \le d \le 1 \\ 4.70 \times DBH_t \times e^{-0.28 \times d}, & 1 < d \le 6.5 \end{cases} \qquad (22)$$

where $TFRB_t$ represents the tree fine root biomass to 2 m depth (t C ha^{-1}) at the year *t*, DBH_t the diameter at breast height (m) at the year *t*, and *d* the distance to the tree (m).

A changing distribution of tree fine roots within the soil profile was taken into account with increasing distance to the tree. For this purpose, exponential functions ($a \times e^{-b \times z}$) were fitted in the alley every 0.5 m distance, and a linear regression was fitted between their coefficients *a* and *b* and distance from the tree. However, the distribution of *TFRB* within the soil profile and with the distance to the tree was considered constant with time.

A decreasing exponential function best represented the changing distribution of tree fine roots within the soil profile with increasing distance to the tree:

$$p_{TFRB,z,d} = \begin{cases} 13.92 \times e^{-1.39 \times z} \quad (R^2 = 0.68), & 0 \le d \le 1 \\ a \times e^{-b \times z}, & 1 < d \le 6.5 \end{cases} \qquad (23)$$

and

$$a = 10.31 - 1.15 \times d \quad (R^2 = 0.69) \qquad (24)$$

$$b = -1.10 + 0.19 \times d \quad (R^2 = 0.51) \qquad (25)$$

Finally,

$$p_{TFRB,z,d} = \begin{cases} 13.92 \times e^{-1.39 \times z}, & 0 \le d \le 1 \\ (10.31 - 1.15 \times d) \times e^{-(-1.10+0.19 \times d) \times z}, & 1 < d \le 6.5 \end{cases} \qquad (26)$$

where $p_{TFRB,z,d}$ is the proportion (%) of the total tree fine root biomass (*TFRB*) at a given depth z (m), and at a distance d from the tree (m).

To finally estimate the tree fine root input due to the mortality, *TFRB* was multiplied by the measured root turnover. The tree fine root turnover ranged from 1.7 to 2.8 yr^{-1} depending on fine root diameter, with an average turnover of 2.2 yr^{-1} for fine roots ≤ 2 mm and to a depth of 2 m (Germon et al., 2016).

2.6.5 Aboveground and belowground input from the crop

As there were more crop yield measurements (14) than straw biomass measurements (6), the effect of agroforestry on the crop yield with time was used as an estimate for change in the aboveground and belowground wheat biomass.

For this, the relative yield ($Rel\ Y_{AF}$) in the agroforestry system was calculated for each year as the ratio between the agroforestry yield and the control yield (Y_C).

The average annual crop yield in the control plot was Y_C = 3.79 ± 0.40 t DM ha^{-1} for the 14 studied years. In the agroforestry plot, the average relative yield decreased linearly with time (increasing *DBH*) and was described using the following linear equation (Fig. 2):

$$Rel\ Y_{AF_t} = -93.33 \times DBH_t + 100 \quad (R^2 = 0.12, \quad p - value = 0.02) \qquad (27)$$

where $Rel\ Y_{AF_t}$ is the average relative crop yield (%) in the agroforestry plot compared to the control plot at year *t*, and DBH_t is the diameter at breast height (m) at year *t*.

The variation of crop yield with distance from the trees was described with a quadratic equation (Fig. 2). But as we aimed to predict SOC stocks up to 6.5 m distance from the trees (middle of the alley), a linear increase of crop yield with increasing distance from the tree gave similar results as the quadratic equation over the 6.5 m distance and was more parsimonious:

$$Rel\ Y_{AF_d} = 4.39 \times d + 64.57 \quad (R^2 = 0.24), \qquad 1 < d \leq 6.5 \qquad (28)$$

where $Rel\ Y_{AF_d}$ is the relative crop yield (%) in the agroforestry plot at a distance d (m) from the tree compared to the control plot.

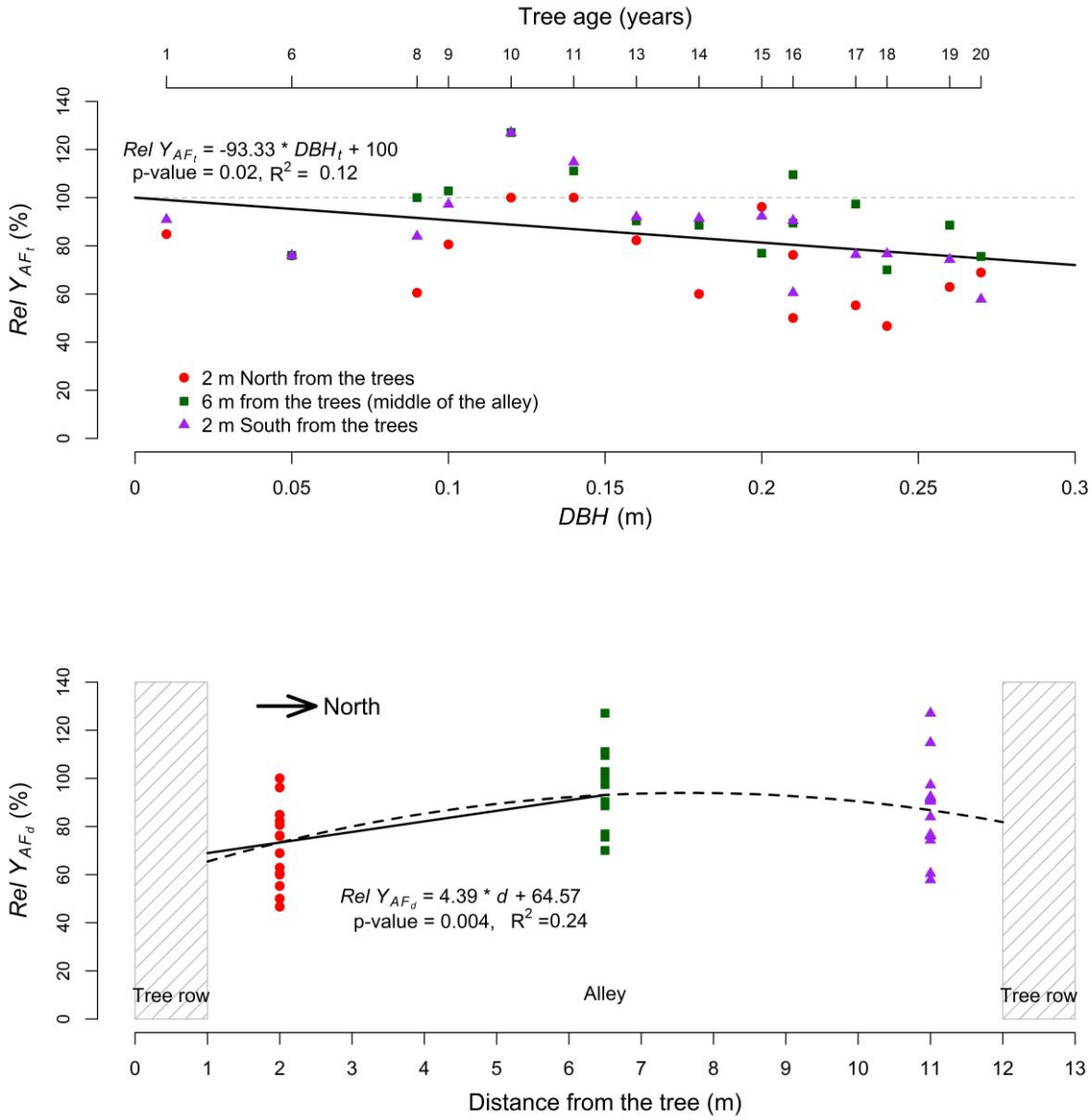

Fig. 2. Top: Relative yield ($Rel\ Y_{AF_t}$) in the agroforestry plot compared to the control plot as a function of tree growth, represented by the diameter at breast height (*DBH*) at year *t*. Bottom: Relative yield ($Y_{AF_{t,d}}$) as a function of the distance from the tree.

Finally, the crop yield in the agroforestry plot was modeled as follows:

$$Y_{AF_{t,d}} = Rel\ Y_{AF_t} \times Y_C \times Rel\ Y_{AF_d} \quad (R^2 = 0.19), \qquad 1 < d \leq 6.5 \qquad (29)$$

where $Y_{AF_{t,d}}$ is the crop yield (t DM ha^{-1}) in the agroforestry plot at the year *t* and at a distance *d* (m) from the tree. Because three linear equations were used to describe the crop yield in the

agroforestry plot, errors were accumulated and we finally came up with a standard underestimation of the crop yield in the agroforestry plot that we corrected by multiplying our equation by 1.2.

The ratio between the straw biomass and the crop yield was calculated as the average of the six measurements, and was considered constant with time. This ratio was used to convert crop yield into straw biomass. In the agroforestry plot, the carbon input to the soil from the aboveground crop biomass was:

$$ABC_{crop,t,d} = Y_{AF_{t,d}} \times (straw\ biomass{:}\ crop\ yield) \times C_{straw} \times (1 - export) \quad (30)$$

where $ABC_{crop,t,d}$ is the aboveground carbon input from the crop (t C ha^{-1}) at the year t and distance d from the tree, $Y_{AF_{t,d}}$ is the agroforestry crop yield. The average ratio between the straw biomass (t DM ha^{-1}) and the crop yield (t DM ha^{-1}) equaled 1.03 ± 0.11 (n=6). The wheat straw was exported out of the field after the harvest, but it was estimated that 25% of the straw biomass was left on the soil, thus *export*=0.75. In the control plot, $Y_{AF_{t,d}}$ was replaced by Y_C.

To estimate fine root biomass of the crop, we hypothesized that the root:shoot ratio of the durum wheat was the same in both the agroforestry and agricultural plot, in the absence of any published data on the matter. In the agroforestry plot, the belowground crop biomass was represented by:

$$BEC_{crop,t,d} = Y_{AF_{t,d}} \times (shoot{:}\ crop\ yield) \times (root{:}\ shoot) \times C_{root} \quad (31)$$

where $BEC_{crop,t,d}$ is the belowground crop biomass (t C ha^{-1}) at the year t and at a distance d from the tree, $Y_{AF_{t,d}}$ is the agroforestry crop yield. The average ratio between the total crop aboveground biomass (*shoot*) and the crop yield equaled 2.45 ± 0.15 (n=6). In 2012, total fine root biomass was 2.29 ± 0.32 t C ha^{-1} in the control (Table 3).

Table 3. Wheat fine root biomass in the agricultural control plot in 2012.

Soil depth (m)	Wheat fine root biomass (kg C m^{-3})	(t C ha^{-1})
0.0-0.1	0.48 ± 0.05	0.48 ± 0.05
0.1-0.3	0.34 ± 0.04	0.69 ± 0.09
0.3-0.5	0.22 ± 0.04	0.44 ± 0.08
0.5-1.0	0.10 ± 0.04	0.52 ± 0.20
1.0-1.5	0.03 ± 0.04	0.17 ± 0.19
Total	-	2.29 ± 0.32

511 Errors represent standard errors.

512

513 Therefore, the wheat *root:shoot* ratio equaled 0.79 ± 0.12 (n=1). The carbon concentration of
514 wheat root was C_{root} = 35.14 ± 1.90 mg C g^{-1}. In the control plot, $Y_{AF_{t,d}}$ was replaced by Y_C.

515

516 In 2012, no wheat roots were observed below 1.5 m, and root biomass decreased exponentially
517 with increasing depth (Table 3). The distribution of crop roots within the soil profile was
518 described as follows:

519 $$p_{CRBc,z} = \begin{cases} 26.44 \times e^{-2.59 \times z} \quad (R^2 = 0.99), & z \leq 1.5 \\ 0, & z > 1.5 \end{cases} \qquad (32)$$

520 where $p_{CRBc,z}$ is the proportion (%) of total crop root biomass in the control plot at a given
521 depth z (m).
522 Since the same maximum rooting depth of the crop was observed in the agroforestry plot and
523 in the control plot, we inferred that the wheat root distribution within the soil profile was not
524 modified by agroforestry, but only its biomass. The crop root turnover was assumed to be 1 yr^{-1}
525 , root mortality occurring mainly after crop harvest.

526

527

528 **2.6.6 Aboveground and belowground input from herbaceous vegetation in the tree rows**

529 The distance from the trees had no effect on the above and belowground biomass of the
530 herbaceous vegetation (data not shown), therefore average values are presented. The summer

aboveground biomass was almost three times higher than in winter, whereas the belowground biomass was two times higher (Table 4). The total aboveground carbon input was 2.13 ± 0.14 t C ha^{-1} yr^{-1} and the total belowground carbon input was 0.74 ± 0.05 t C ha^{-1} yr^{-1} to 0.5 m depth.

Table 4. Aboveground and belowground biomass of the herbaceous vegetation in the tree rows.

		Herbaceous biomass (t C ha^{-1})	
	Soil depth (m)	Summer	Winter
Aboveground	-	1.57 ± 0.11	0.56 ± 0.09
Belowground	0.0-0.1	0.22 ± 0.03	0.17 ± 0.01
	0.1-0.3	0.16 ± 0.02	0.06 ± 0.01
	0.3-0.5	0.09 ± 0.04	0.04 ± 0.01
	Total	0.46 ± 0.04	0.27 ± 0.02

Errors represent standard errors.

The belowground carbon input from the tree row vegetation ($BEC_{veg,z}$, t C ha^{-1}) at a given depth z (m) was described by the following equation:

$$BEC_{veg,z} = \begin{cases} 0.44 \times e^{-3.12 \times z}, & z \leq 1.5 \\ 0, & z > 1.5 \end{cases} \quad (33)$$

We assumed for simplification that the aboveground and belowground biomasses of the herbaceous vegetation in the tree row were constant over time.

2.7 Optimization procedure

Depending on the model variant, four to five parameters were optimized with a Bayesian statistical method (Santaren et al., 2007; Tarantola, 1987, 2005) using measured SOC stocks from the control plot only. These parameters were A, the advection rate, D, the diffusion coefficient, h the humification yield, a the coefficient of the k_{HSOC} rate from Eq. (10), and PE the priming coefficient. These four or five parameters were calibrated so that equilibrium SOC stocks, i.e. after 5000 years of simulation, equaled SOC stocks of the control plot in 2013. The associated uncertainty was estimated with the 93 soil cores sampled in the control plot (see

552 section 2.2.1). Due to a lack of relevant data, we assumed that the climate and the land use were
553 the same for the last 5000 years, and that SOC stocks in the control plot were at equilibrium at
554 the time of measurement. Therefore, SOC stocks at the end of the 5000 years of simulation
555 equaled SOC stocks in the control plot. Three different calibrations were performed,
556 corresponding to the three different models that were used: one calibration with the two pools
557 model without the priming effect, one calibration with the two pools model with the priming
558 effect, and one calibration with the three pools model.
559 Each model variant was fitted to the control SOC stocks data using a Bayesian curve fitting
560 method described in Tarantola (1987), after a conversion from SOC stocks in kg C m^{-2} to SOC
561 stocks in kg m^{-3} due to the different soil layers' thickness. We aimed to find a parameter set
562 that minimizes the distance between model outputs and the corresponding observations,
563 considering model and data uncertainties, and prior information on parameters. With the
564 assumption of Gaussian errors for both the observations and the prior parameters, the optimal
565 parameter set corresponds to the minimum of the cost function $\boldsymbol{J}(\boldsymbol{x})$:

566 $$\boldsymbol{J}(\boldsymbol{x}) = 0.5 \times \left[(\boldsymbol{y} - \boldsymbol{H}(\boldsymbol{x}))^t \times \boldsymbol{R}^{-1} \times \left(\boldsymbol{y} - \boldsymbol{H}(\boldsymbol{x})\right) + (\boldsymbol{x} - \boldsymbol{x}_b)^t \times {\boldsymbol{P}_b}^{-1} \times (\boldsymbol{x} - \boldsymbol{x}_b)\right] \quad (34)$$

567 that contains both the mismatch between modelled and observed SOC stock and the mismatch
568 between a priori and optimized parameters. $\boldsymbol{x}$ is the vector of unknown parameters, $\boldsymbol{x}_b$ the
569 vector of a priori parameter values, $\boldsymbol{H()}$ the model and y the vector of observations. The
570 covariance matrices $\boldsymbol{P}_b$ and $\boldsymbol{R}$ describe a priori uncertainties on parameters, and observations,
571 respectively. Both matrices are diagonal as we suppose the observation uncertainties and the
572 parameter uncertainties to be independent. To determine an optimal set of parameters which
573 minimizes $\boldsymbol{J}(\boldsymbol{x})$, we used the BFGS gradient-based algorithm (Tarantola, 1987). For each model
574 variant, we performed 30 optimizations starting with different parameter prior values to check
575 that the results did not correspond to a local minimum. As the BFGS algorithm does not directly

calculate the variance of posteriors, they were quantified using the curvature cost function at its minimum once it was reached (Santaren et al., 2007).

2.8 Comparison of models

Model predictions with and without priming effect were compared calculating the coefficients of determination, root mean square errors (RMSE) and Bayesian information criteria (BIC).

$$RMSE = \sqrt{\frac{1}{N}\sum_{i=1}^{N}(x_i - \bar{x})^2} \qquad (35)$$

where i is the number of observations (1 to N), x_i is the predicted value and $\bar{x}$ is the mean observed value.

$$BIC = k \times \ln(N) - 2 \times ln(\hat{L}) \qquad (36)$$

where N is the number of observations, k is the number of model parameters, and $\hat{L}$ is the maximized value of the likelihood function of the model (Schwarz, 1978).

The model was run at a yearly time step using mean annual soil temperature and moisture and annual C inputs to the soil. In the agroforestry, the model was run from the ground (0 m) to 2 m depth, and from the tree (0 m) to 6.5 m from the tree (middle of the alley). The model was applied separately across locations of a tree-distance gradient having varying OC inputs, each soil column was considered independent from another. SOC pools were initialized after a spin-up of 5000 years in the control plot. At t_0, SOC stocks in the agroforestry plot therefore equaled SOC stocks of the control plot. The model was then run from t_0 to t_{18} (years) after tree planting. The spatial resolution was 0.1 m both vertically and horizontally. The model was developed using R 3.1.1 (R Development Core Team, 2013). Partial-differential equations were solved using the R package *deSolve* and the *ode.1D* method (Soetaert et al., 2010).

3 Results

3.1 Organic carbon inputs and SOC stocks: a synthesis from field measurements

In the alleys of the18-year-old agroforestry system, measured organic carbon (OC) inputs from the crop residues and roots were reduced compared to the control plot due a lower crop yield (Fig. 3). This reduction in crop OC inputs was offset by OC inputs from the tree roots and tree litterfall. Total root OC inputs in the alleys (crop + tree roots) and in the control plot (crop roots) were very similar, respectively 2.43 and 2.29 t C ha^{-1} yr^{-1}. Alleys received 0.60 t C ha^{-1} yr^{-1} more of total aboveground biomass (crop residues + tree litterfall) than the control, which was added to the plough layer. Tree rows received 2.35 t C ha^{-1} yr^{-1} more C inputs in the first 0.3 m of soil compared to the control plot, mainly from the herbaceous vegetation. Down the whole soil profile, tree rows received two times more OC inputs compared to the control plot (Fig. 3), and 65% more than alleys. Overall, the agroforestry plot had 41% more OC inputs to the soil than the control plot to 2 m depth (3.80 t C ha^{-1} yr^{-1} compared to 2.69 t C ha^{-1} yr^{-1}). In the agroforestry plot, the largest aboveground OC input to the soil comes from the herbaceous vegetation, and not from the trees. In the control plot, 85% of OC inputs are wheat root litters. In the agroforestry plot, root inputs represent 71% of OC inputs in the alleys, and 50% in the tree rows.

In the first 0.3 m of soil, SOC stocks were significantly higher in the alleys than in the control plot, but the difference was small (2.1 ± 0.6 t C ha^{-1}). Between 0.3 and 1.0 m, the difference of SOC stocks was smaller but still significant. However, between 1 and 2 m depth, SOC stocks were significantly lower in the alleys than in the control. As a consequence, there was no significant difference of total SOC stocks between the two locations down the whole soil profile. In the tree rows, topsoil organic carbon stocks (0.0-0.3 m) were much higher than in the control (+ 17.0 ± 1.4 t C ha^{-1}). This positive difference of SOC stocks decreased with depth

but remained significantly positive down 1.5 m depth. The opposite was observed between 1.5 and 2.0 m depth. Delta of total SOC stocks between the tree rows and the control plot was 20.1 ± 1.6 t C ha^{-1}. At the plot scale, total SOC stocks were significantly higher in the agroforestry plot compared to the control plot down 2 m depth (+ 3.3 ± 0.9 t C ha^{-1}).

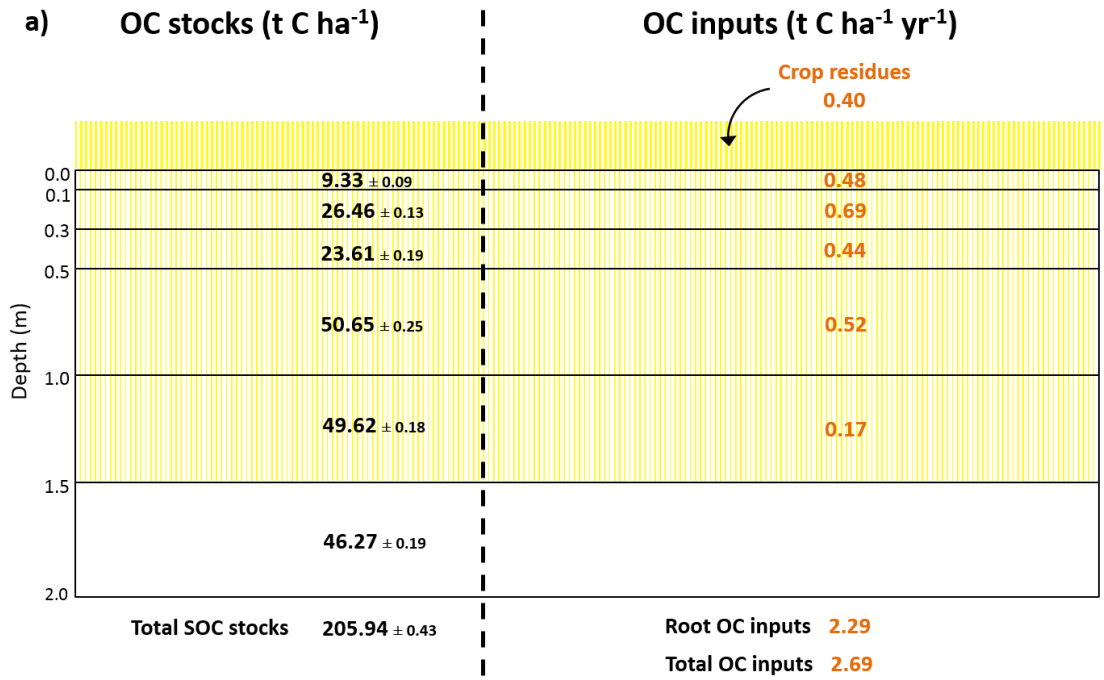

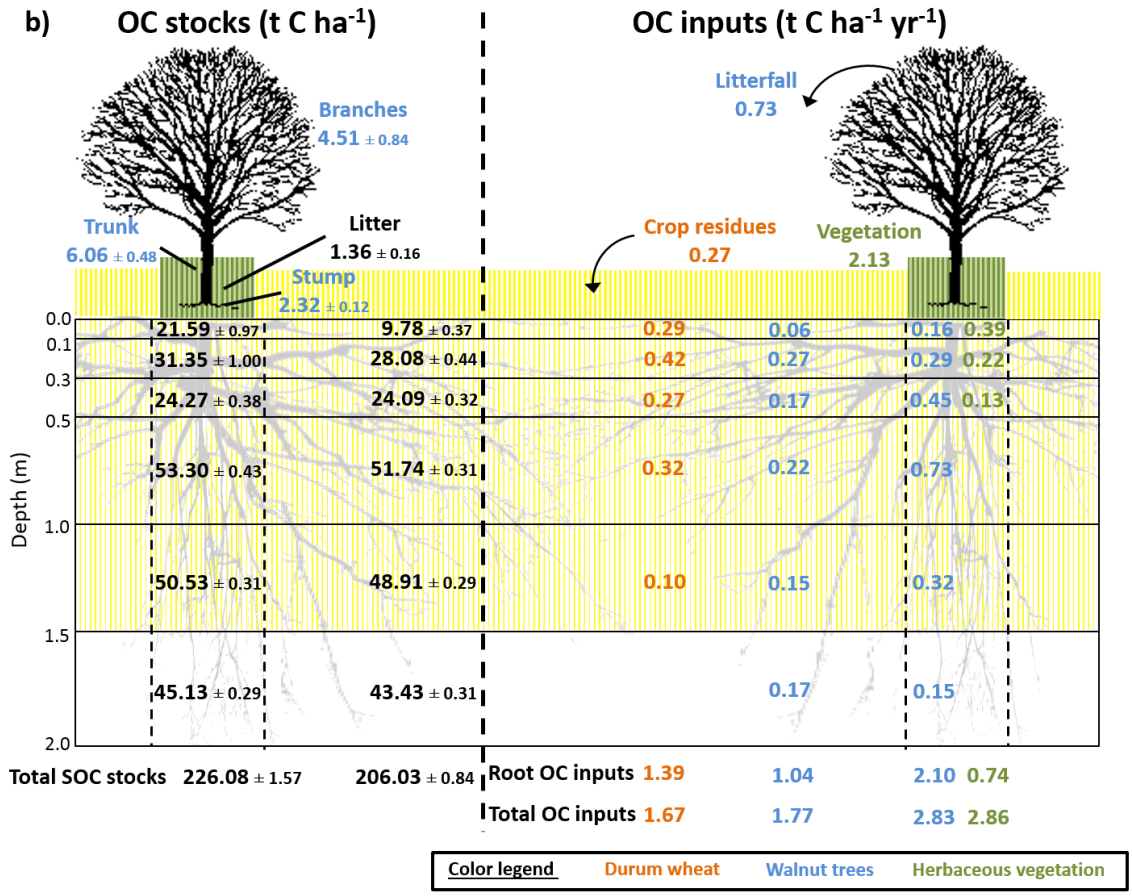

Fig. 3. Measured soil organic carbon stocks and organic carbon inputs to the soil a) in the agricultural control plot, b) in the 18-year-old agroforestry plot. Associated errors are standard errors. Values are expressed per hectare of land type (control, alley, tree row). To get the values per hectare of agroforestry, data from alley and tree row have to be weighted by their respective surface area (i.e., 84% and 16%, respectively) and then added up. OC: organic carbon; SOC: soil organic carbon. SOC stocks data are issued from Cardinael *et al.*, (2015a), data of tree root OC inputs are combined from Cardinael *et al.*, (2015b) and from Germon *et al.*, (2016).

3.2 HSOC decomposition rate

The soil incubation experiment showed that the HSOC mineralization rate decreased exponentially with depth (Fig. S1) and could be described with:

643 $$k_{HSOC,z} = 6.114 \times e^{-1.37 \times z} \quad (R^2 = 0.76) \qquad (37)$$

644 where z is the soil depth (m), and where the *a* (yr^{-1}) coefficient (*a* = 6.114) was further optimized

645 (Table 5).

646

Table 5. Summary of optimized model parameters.

Model parameter	Meaning	Prior range (log)*	Posterior values ± variance (prior values)		
			2 pools - without *PE*	2 pools - with *PE*	3 pools – without *PE*
a	coefficient from Eq. (8) of the HSOC decomposition (yr^{-1})	-12.52-1.29	$0.01e^{-2} \pm <10^{-4}$ ($0.01e^{-2}$)	$0.01e^{-2} \pm <10^{-4}$ ($0.01e^{-2}$)	-
a_1	coefficient from Eq. (8) of the HSOC1 decomposition (yr^{-1})	-12.52-1.29	-	-	$0.01e^{-2} \pm <10^{-4}$ ($0.01e^{-2}$)
a_2	coefficient from Eq. (8) of the HSOC2 decomposition (yr^{-1})	-12.52-1.29	-	-	$0.83e^{-2} \pm 0.17e^{-2}$ ($0.83e^{-2}$)
D	diffusion coefficient ($cm^2\ yr^{-1}$)	-13.82-0	$4.62e^{-4} \pm 5.95e^{-4}$ ($9.64e^{-4}$)	$5.63e^{-4} \pm 1.42e^{-4}$ ($9.01e^{-4}$)	$5.24e^{-4} \pm 7.62e^{-4}$ ($9.64e^{-4}$)
A	advection rate ($mm\ yr^{-1}$)	-13.82-0	$21.25e^{-4} \pm 5.02e^{-4}$ ($8.54e^{-4}$)	$6.63e^{-4} \pm 2.38e^{-4}$ ($4.27e^{-4}$)	$21.60e^{-4} \pm 2.24e^{-4}$ ($8.54e^{-4}$)
h	humification yield	-4.61-0	$0.32 \pm <10^{-4}$ (0.34)	$0.25 \pm 1.00e^{-4}$ (0.13)	0.34 ± 0.03 (0.34)
PE	priming coefficient	-2.30-5.08	-	9.66 ± 1.49 (102.95)	-
f_1	fraction of decomposed FOC entering the HSOC1 pool	0-1	-	-	0.99 ± 0.18 (0.86)
f_2	fraction of decomposed HSOC1 entering the FOC pool	0-1	-	-	$0.94 \pm 1.10e^{-3}$ (0.80)

The prior range represents the range in which prior values were sampled for the 30 optimizations per model variant. The prior values presented in brackets in the posterior column represent the prior values that minimized the **J(x)** value (Eq. (34)). * Except for f_1 and f_2.

3.3 Modeling results

3.3.1 Optimized parameters and correlation matrix

The optimized parameters and their prior modes are presented in Table 5. For the two pools model without priming effect, the most important correlation was observed between *h* and *A* which control the humification and the transport by advection. Concerning the two pools model with priming effect, the most important correlations were observed between *h* and *PE* which controls the effect of the FOC on HSOC decomposition, and between *h* and *A*. *A* and *PE* were also positively correlated (Fig. S2). For the three pools model, f_1 and f_2 were by definition negatively correlated, but f_2 and *A* were also correlated. Considering the method used to optimize the parameters, these important correlation factors hinder the presentation of the model output within an envelope. Therefore, we presented the model results using the optimized parameter without any envelope.

3.3.2 Modeled SOC stocks

As a reminder, SOC stocks of the agroforestry plot were not part of model calibration (that used the control plot only) but were used here for validation. Observed SOC stocks were not well represented by the two pools model without priming effect, with RMSE ranging from 1.00 to 1.07 kg C m^{-3} (Fig. 4, Table S2). The model performed better when the priming effect was taken into account, with RMSE ranging from 0.41 to 0.95 kg C m^{-3}, and the SOC profile was well described. The representation of SOC stocks was not improved by the inclusion of a third C pool in the model. Overall, the two pools model with priming effect was the best one, as shown by the BICs (Fig. 4, Table S2). For all models, SOC stocks below 1 m depth were better described than above SOC stocks (Table S2). The spatial distribution of SOC stocks and of additional SOC storage was also well described (Fig. 5), with a very high additional SOC storage in the topsoil layer in the tree row. Most modeled SOC storage in the agroforestry plot

was located in the first 0.2 m depth, but SOC storage was slightly higher in the middle of the alleys than in the alleys close to the tree rows.

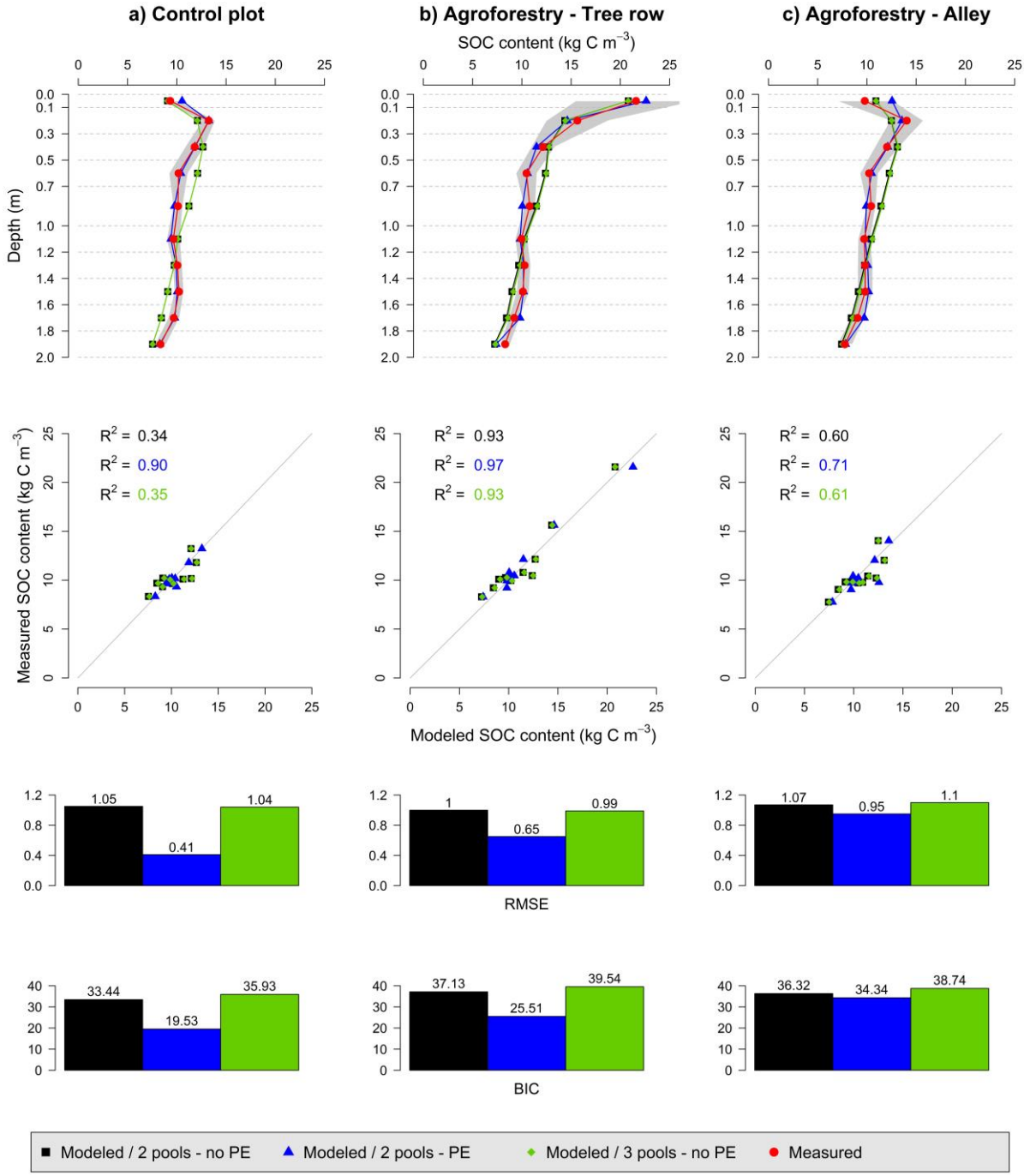

Fig. 4. Measured and modeled soil organic carbon contents (kg C m^{-3}) in an agricultural control plot and in an 18-year-old silvoarable system with a two pools model without priming effect (no *PE*), with a two pools model with priming effect (*PE*) and with a three pools model without

PE. Gray shaded bands represent standard deviations of measured SOC stocks (n=93 in the control, n=40 in the tree rows, and n=60 in the alleys).

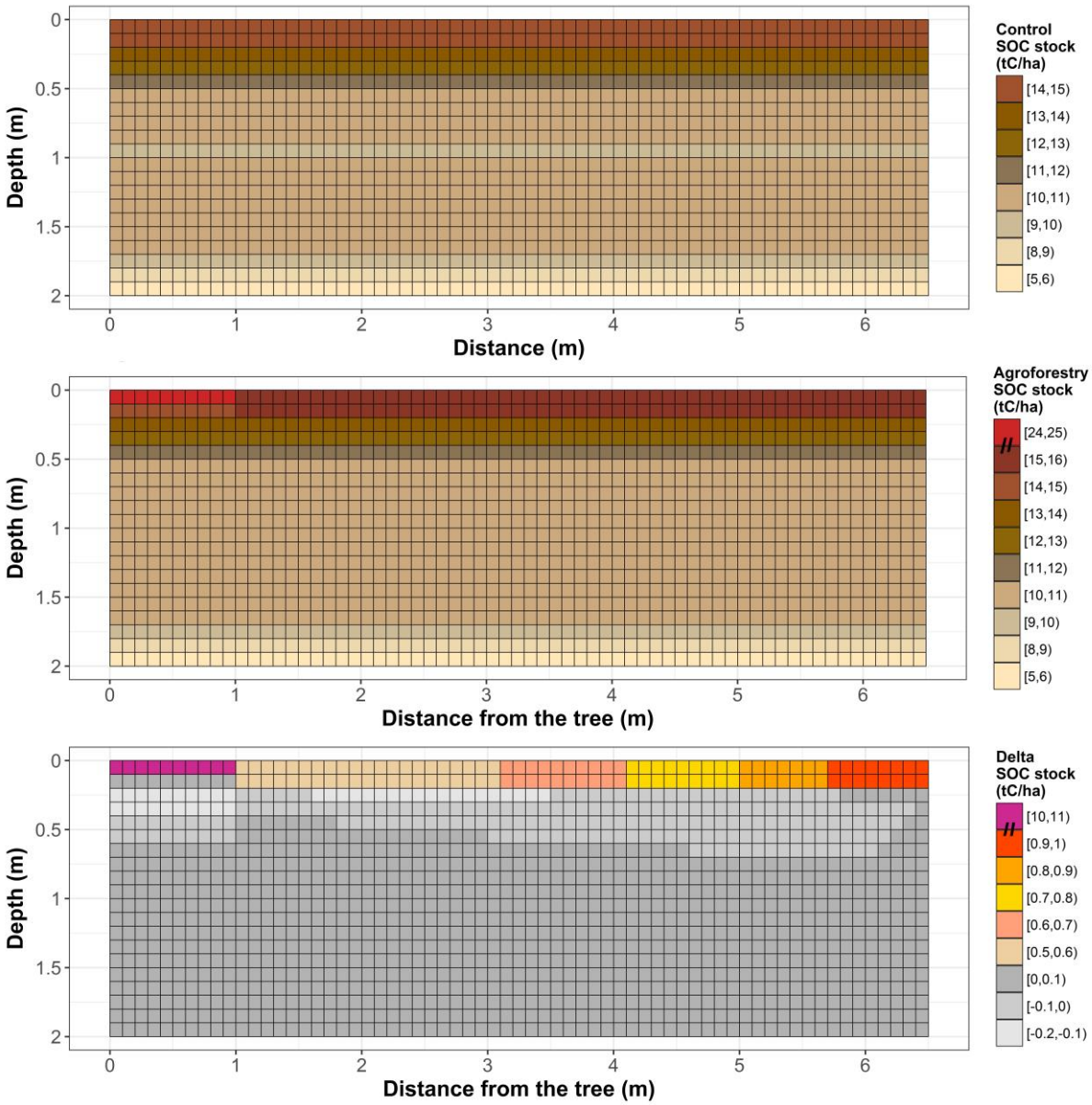

Fig. 5. Spatial distribution of control SOC stocks (top), agroforestry SOC stocks (middle), and additional SOC storage (t C ha^{-1}) in an 18-year-old silvoarable system compared to an agricultural control plot and represented by the two pools model with priming effect. The scale used in the middle and bottom panels are not continuous due to the large stocks predicted by the model in the top layer in the tree-row.

690

691 **4 Discussion**

692 **4.1 OC inputs drive SOC storage in agroforestry systems**

693 Increased SOC stocks in the agroforestry plot compared to the control may be explained either
694 by increased OC inputs, or decreased OC outputs by SOC mineralization, or both. In the alleys,
695 higher SOC stocks in the topsoil could be explained by inputs from litterfall and tree roots
696 despite a decrease in crop inputs. Most of additional SOC storage in the agroforestry plot was
697 found in the topsoil in the tree rows. The same distribution was observed for OC inputs to the
698 soil. Inputs from the herbaceous vegetation had an important impact on SOC storage. The
699 increased SOC stocks in the tree rows were largely explained by an important above-ground
700 carbon input (2.13 t C ha^{-1} yr^{-1}) by the herbaceous vegetation between trees. This result had
701 already been suggested by Cardinael et al., (2015b) and by Cardinael et al., (2017) who showed
702 that even young agroforestry systems could store SOC in the tree rows while trees are still very
703 small. These "grass strips" indirectly introduced by the tree planting in parallel tree rows have
704 a major impact on SOC stocks of agroforestry systems. Increased SOC stocks below the plough
705 layer could be explained by higher root inputs, but these inputs could also have contributed to
706 decrease SOC stocks below 1.5 m due to priming effect. At the plot scale, measured organic
707 carbon inputs to the soil were increased by 40% (+1.1 t C ha^{-1} yr^{-1}) down 2 m depth in the 18-
708 year-old agroforestry plot compared to the control plot, resulting in increased SOC stocks of
709 3.3 t C ha^{-1}. Increased OC inputs in agroforestry systems has been shown in other studies but
710 they were only quantified in the first 20 cm of soil (Oelbermann et al., 2006; Peichl et al., 2006).
711 This study is therefore the first one also quantifying deep OC inputs to soil. In this study and
712 due to a lack of data, soil temperature and soil moisture were considered the same in both plots
713 so that abiotic factors controlling SOC decomposition were identical. Reduced soil temperature
714 is often observed in agroforestry systems (Clinch et al., 2009; Dubbert et al., 2014), but effect

of agroforestry on soil moisture is much more complex. The soil evaporation is reduced under the trees, but soil water is also lost through the transpiration of trees (Ilstedt et al., 2016; Ong and Leakey, 1999). These opposing effects vary with the distance from the tree (Odhiambo et al., 2001). Moreover, increased water infiltration and water storage has been observed under the trees after a rainy event (Anderson et al., 2009). Therefore, the effect of agroforestry on soil moisture is variable in time and space, and should be investigated more in details. Interactions between soil temperature and soil moisture on the SOC decomposition are known to be complex (Conant et al., 2011; Moyano et al., 2013; Sierra et al., 2015). A sensitivity analysis performed on these two boundary conditions showed that the model was not very sensitive to soil temperature and soil moisture (Fig. S3), but the real effect of these two parameters on SOC dynamics under agroforestry systems should be specifically investigated in future studies. Despite these simplifying assumptions on similarities in microclimate but also on vertical transport between the control and the agroforestry system, the model calibrated to the control plot was able to reproduce SOC stocks in tree rows and alleys and its depth distribution well. This strong validation also revealed that OC inputs were sufficient to explain the differences in SOC stocks at this site. Furthermore, the SOC decomposition rate could also be modified due to an absence of soil tillage in the tree rows (Balesdent et al., 1990) or to an increased aggregate stability (Udawatta et al., 2008) in the topsoil.

4.2 Representation of SOC spatial heterogeneity in agroforestry systems

The lateral spatial heterogeneity of SOC stocks in the agroforestry plot was well described by the two pools model including priming effect, with higher SOC stocks in the tree rows' topsoil than in the alleys. The model treated the carbon from the tree row herbaceous litter as an input to the upper layer of the mineral soil, in the same way as inputs by roots. Introduction of nitrogen in the model could be further tested in order to take into account a lower carbon use

efficiency due to a lack of nutrients for microbial growth in this litter. For all models, SOC stocks were better described in the tree rows than in the alleys. In the alleys, the spatial distribution of organic inputs is more complex and thus more difficult to model. The tree root system is influenced by the soil tillage and by the competition with the crop roots, and thus the highest tree fine root density is not observed in the topsoil but in the 0.3-0.5 m soil layer (Cardinael et al., 2015a). In the model, we were not able to represent this specific tree root pattern with commonly used mathematical functions, and tree root profiles were modeled, by default, using a decreasing exponential. Indeed, piecewise linear functions introduce threshold effects not desirable for transport mechanisms, especially diffusion. This simplification could partly explain the model overestimation of SOC stocks in the 0.0-0.1 m layer of the alleys compared to observed data. This result suggests that it could be useful to couple the CARBOSAF model with a model describing root architecture and root growth (Dunbabin et al., 2013; Dupuy et al., 2010), using for instance voxel automata (Mulia et al., 2010). Moreover, the model described a slight increase of SOC stocks in the middle of the alleys than close to the trees in the alleys. This could be explained by the linear equation used to describe the crop yield as a function of the distance from the trees, leading to an overestimation of the crop yield reduction close to the trees. It could also be explained by the formalism used to model leaf litter distribution in the plot. We considered a homogeneous distribution of leaf inputs in the agroforestry plot, which was the case in the last years, but probably not in the first years of the tree growth where leaves might be more concentrated close to the trees (Thevathasan and Gordon, 1997).

The two pools model with priming effect also represented a slight SOC storage in the agroforestry plot below 1.0 m depth, but it was not observed in the field. This could be linked to an overestimation of C input from tree fine root mortality. Indeed, a constant root turnover was considered along the soil profile, but several authors reported a decrease of the root

turnover with increasing soil depth (Germon et al., 2016; Hendrick and Pregitzer, 1996; Joslin et al., 2006). However, the sensitivity analysis showed that the model was not sensitive to this parameter (Fig. S3).

4.3 Vertical representation of SOC profiles in models

The best model to represent SOC profiles considered the priming effect. This process can act in two different ways on the shape of SOC profiles. It has a direct effect on the SOC mineralization and it therefore modulates the amount of SOC in each soil layer, creating different SOC gradients. This indirectly affects the mechanisms of C transport within the soil profile, as shown by a modification of transport coefficients in the case of priming effect (Table 5). Contrary to what was shown by Cardinael *et al.*, (2015c) in long term bare fallows receiving contrasted organic amendments, the addition of another SOC pool could not surpass the inclusion of priming effect in terms of model performance. Together with Wutzler & Reichstein, (2013) and Guenet *et al.*, (2016), this study therefore suggests that implementing priming effect into SOC models would improve model performances especially when modelling deep SOC profiles.

We considered here the same transport coefficients for the FOC and HSOC pools, but the quality and the size of OC particles are different, potentially leading to various movements in the soil by water fluxes or fauna activity (Lavelle, 1997). Moreover, we considered identical transport parameters in the agroforestry and in the control plot, but the presence of trees could modify soil structure, soil water fluxes (Anderson et al., 2009), and the fauna activity (Price and Gordon, 1999). However, the model was little sensitive to these parameters (Fig. S3). Further study could investigate the role of different transport coefficients on the description of SOC profiles.

4.4 Higher OC inputs or a different quality of OC?

The introduction of trees in an agricultural field not only modifies the amount of litter residues, but also their quality. Tree leaves, tree roots, and the herbaceous vegetation from the tree row have different C:N ratios, lignin and cellulose contents than the crop residues. Recent studies showed that plant diversity had a positive impact on SOC storage (Lange et al., 2015; Steinbeiss et al., 2008). One of the hypothesis proposed by the authors is that diverse plant communities result in more active, more abundant and more diverse microbial communities, increasing microbial products that can potentially be stabilized. In our model, litter quality is not related to different SOC pools, but is implicitly taken into account in the FOC decomposition rate, which is weighted by the respective contribution from the different types of OC inputs. To test this, we performed a model run considering that all OC inputs in the agroforestry plot were crop inputs (all FOC decomposition rates equaled wheat decomposition rate), but results were not significantly different from the one presented here. Hence, we considered that changes in litter quality in the agroforestry plot did not significantly influence SOC decomposition rates.

4.5 Possible limitation of SOC storage by priming effect

Our modelling results suggested that the priming effect could considerably reduce the capacity of soils to store organic carbon. Our study showed that the increase of SOC stocks was not proportional to OC inputs, especially at depth. This result has often been observed in Free Air CO_2 Enrichment (FACE) experiments. In these experiments, productivity is usually increased due to CO_2 fertilization, but several authors also reported an increase in SOC decomposition but not linearly linked to the productivity increase (van Groenigen et al., 2014; Sulman et al., 2014). In a long-term FACE experiment, Carney *et al.*, (2007) also found that SOC decreased due to priming effect, offsetting 52% of additional carbon accumulated in aboveground and coarse root biomass. The priming effect intensity also relies on nutrient availability (Zhang et

al., 2013). In agroforestry systems, tree roots can intercept leached nitrate below the crop rooting zone (Andrianarisoa et al., 2016), reducing nutrient availability. This beneficial ecosystem service could indirectly increase the priming effect intensity in deep soil layers.

The formalism used here to simulate priming effect assumes that there is no mineralisation of the SOC in the absence of fresh OC inputs (no basal respiration). This is a strong hypothesis, but this situation never occurs since the FOC pool is never empty (data not shown). In the alleys and below the maximum rooting depth of crops, there are no direct inputs of FOC, but OC is transported in these deep layers due to transport mechanisms. However, further studies could study the impact of the priming effect formalism on the estimation of its intensity by using explicit microbial biomass for instance (Blagodatsky et al., 2010; Perveen et al., 2014).

Finally, root exudates were not quantified in this study. Several authors showed that they could induce strong priming effects (Bengtson et al., 2012; Keiluweit et al., 2015), but root exudates are also a source of labile carbon, potentially contributing to stable SOC (Cotrufo et al., 2013). These opposing effects of root exudates on SOC should be further investigated, especially concerning the deep roots in agroforestry systems.

5 Conclusions

We proposed the first model that simulates soil organic carbon dynamics in agroforestry accounting for both the whole soil profile and the lateral spatial heterogeneity in agroforestry plots. The two pools model with priming effect described reasonably well the measured SOC stocks after 18 years of agroforestry and SOC distributions with depth. It showed that the increased inputs of fresh biomass to soil in the agroforestry system explained the observed additional SOC storage and suggested priming effect as a process controlling SOC stocks in the presence of trees. This study points out at processes that may be modified by deep rooting trees

and deserve further studies given their potential effects on SOC dynamics, such as additional inputs of C as roots exudates, or altered soil structure leading to modified SOC transport rates.

6 Data availability

The data and the model are freely available upon request and can be obtained by contacting the author (remi.cardinael@cirad.fr).

Information about the Supplement

The Supplement includes the walnut tree fine root biomass (Table S1), the different model performances (Table S2), the potential SOC decomposition rate as a function of soil depth (Fig. S1), the correlation matrix of optimized parameters (Fig. S2), and a sensitivity analysis of the model (Fig. S3).

Acknowledgments.

This study was financed by the French Environment and Energy Management Agency (ADEME), following a call for proposals as part of the REACCTIF program (Research on Climate Change Mitigation in Agriculture and Forestry). This work was part of the funded project AGRIPSOL (Agroforestry for Soil Protection, 1260C0042), coordinated by Agroof. Rémi Cardinael was supported both by ADEME and by La Fondation de France. We thank the farmer, Mr Breton, who allowed us to sample in his field. We are very grateful to our colleagues for their work in the field since the tree planting, especially Jean-François Bourdoncle, Myriam Dauzat, Lydie Dufour, Jonathan Mineau, Alain Sellier and Benoit Suard. We thank colleagues and students who helped us for measurements in the field or in the laboratory, especially Daniel Billiou, Cyril Girardin, Patricia Mahafaka, Agnès Martin, Valérie Pouteau, Alexandre Rosa,

and Manon Villeneuve. Finally, we would like to thank Jérôme Balesdent, Pierre Barré and Philippe Peylin for their valuable comments on the modeling part of this work.

References

Ahrens, B., Braakhekke, M. C., Guggenberger, G., Schrumpf, M. and Reichstein, M.: Contribution of sorption, DOC transport and microbial interactions to the ^{14}C age of a soil organic carbon profile: Insights from a calibrated process model, Soil Biol. Biochem., 88, 390–402.

Albrecht, A. and Kandji, S. T.: Carbon sequestration in tropical agroforestry systems, Agric. Ecosyst. Environ., 99, 15–27, 2003.

Anderson, S. H., Udawatta, R. P., Seobi, T. and Garrett, H. E.: Soil water content and infiltration in agroforestry buffer strips, Agrofor. Syst., 75(1), 5–16, 2009.

Andrianarisoa, K., Dufour, L., Bienaime, S., Zeller, B. and Dupraz, C.: The introduction of hybrid walnut trees (*Juglans nigra* x *regia* cv. NG23) into cropland reduces soil mineral N content in autumn in southern France, Agrofor. Syst., 90(2), 193–205, 2016.

Baisden, W. T. and Parfitt, R. L.: Bomb ^{14}C enrichment indicates decadal C pool in deep soil?, Biogeochemistry, 85, 59–68, 2007.

Baisden, W. T., Amundson, R., Brenner, D. L., Cook, A. C., Kendall, C. and Harden, J. W.: A multiisotope C and N modeling analysis of soil organic matter turnover and transport as a function of soil depth in a California annual grassland soil chronosequence, Global Biogeochem. Cycles, 16(4), 82-1-82–26, 2002.

Balandier, P. and Dupraz, C.: Growth of widely spaced trees. A case study from young agroforestry plantations in France, Agrofor. Syst., 43, 151–167, 1999.

Balesdent, J., Mariotti, A. and Boisgontier, D.: Effect of tillage on soil organic carbon

887 mineralization estimated from ^{13}C abundance in maize fields, J. Soil Sci., 41(4), 587–596, 1990.

888 Bambrick, A. D., Whalen, J. K., Bradley, R. L., Cogliastro, A., Gordon, A. M., Olivier, A. and
889 Thevathasan, N. V: Spatial heterogeneity of soil organic carbon in tree-based intercropping
890 systems in Quebec and Ontario, Canada, Agrofor. Syst., 79, 343–353, 2010.

891 Bengtson, P., Barker, J. and Grayston, S. J.: Evidence of a strong coupling between root
892 exudation, C and N availability, and stimulated SOM decomposition caused by rhizosphere
893 priming effects, Ecol. Evol., 2(8), 1843–1852, 2012.

894 Blagodatsky, S., Blagodatskaya, E., Yuyukina, T. and Kuzyakov, Y.: Model of apparent and
895 real priming effects: Linking microbial activity with soil organic matter decomposition, Soil
896 Biol. Biochem., 42(8), 1275–1283, 2010.

897 Braakhekke, M. C., Beer, C., Hoosbeek, M. R., Reichstein, M., Kruijt, B., Schrumpf, M. and
898 Kabat, P.: SOMPROF: A vertically explicit soil organic matter model, Ecol. Modell., 222(10),
899 1712–1730, 2011.

900 Bruun, S., Christensen, B. T., Thomsen, I. K., Jensen, E. S. and Jensen, L. S.: Modeling vertical
901 movement of organic matter in a soil incubated for 41 years with ^{14}C labeled straw, Soil Biol.
902 Biochem., 39(1), 368–371, 2007.

903 Burgess, P. J., Incoll, L. D., Corry, D. T., Beaton, A. and Hart, B. J.: Poplar (*Populus* spp)
904 growth and crop yields in a silvoarable experiment at three lowland sites in England, Agrofor.
905 Syst., 63, 157–169, 2004.

906 Cardinael, R., Mao, Z., Prieto, I., Stokes, A., Dupraz, C., Kim, J. H. and Jourdan, C.:
907 Competition with winter crops induces deeper rooting of walnut trees in a Mediterranean alley
908 cropping agroforestry system, Plant Soil, 391, 219–235, 2015a.

909 Cardinael, R., Chevallier, T., Barthès, B. G., Saby, N. P. A., Parent, T., Dupraz, C., Bernoux,
910 M. and Chenu, C.: Impact of alley cropping agroforestry on stocks, forms and spatial

911 distribution of soil organic carbon - A case study in a Mediterranean context, Geoderma, 259–
912 260, 288–299, 2015b.

913 Cardinael, R., Eglin, T., Guenet, B., Neill, C., Houot, S. and Chenu, C.: Is priming effect a
914 significant process for long-term SOC dynamics? Analysis of a 52-years old experiment,
915 Biogeochemistry, 123, 203–219, 2015c.

916 Cardinael, R., Chevallier, T., Cambou, A., Béral, C., Barthès, B. G., Dupraz, C., Durand, C.,
917 Kouakoua, E. and Chenu, C.: Increased soil organic carbon stocks under agroforestry: A survey
918 of six different sites in France, Agric. Ecosyst. Environ., 236, 243–255, 2017.

919 Carney, K. M., Hungate, B. A., Drake, B. G. and Megonigal, J. P.: Altered soil microbial
920 community at elevated CO_2 leads to loss of soil carbon, PNAS, 104(12), 4990–4995, 2007.

921 Charbonnier, F., le Maire, G., Dreyer, E., Casanoves, F., Christina, M., Dauzat, J., Eitel, J. U.
922 H., Vaast, P., Vierling, L. A. and Roupsard, O.: Competition for light in heterogeneous
923 canopies: Application of MAESTRA to a coffee (*Coffea arabica* L.) agroforestry system,
924 Agric. For. Meteorol., 181, 152–169, 2013.

925 Chaudhry, A. K., Khan, G. S., Siddiqui, M. T., Akhtar, M. and Aslam, Z.: Effect of arable crops
926 on the growth of poplar (*Populus deltoides*) tree in agroforestry system, Pakistan J. Agric. Sci.,
927 40, 82–85, 2003.

928 Chifflot, V., Bertoni, G., Cabanettes, A. and Gavaland, A.: Beneficial effects of intercropping
929 on the growth and nitrogen status of young wild cherry and hybrid walnut trees, Agrofor. Syst.,
930 66(1), 13–21, 2006.

931 Clinch, R. L., Thevathasan, N. V., Gordon, A. M., Volk, T. A. and Sidders, D.: Biophysical
932 interactions in a short rotation willow intercropping system in southern Ontario, Canada, Agric.
933 Ecosyst. Environ., 131(1–2), 61–69, 2009.

934 Conant, R. T., Ryan, M. G., Ågren, G. I., Birge, H. E., Davidson, E. A., Eliasson, P. E., Evans,

S. E., Frey, S. D., Giardina, C. P., Hopkins, F. M., Hyvönen, R., Kirschbaum, M. U. F., Lavallee, J. M., Leifeld, J., Parton, W. J., Megan Steinweg, J., Wallenstein, M. D., Martin Wetterstedt, J. Å. and Bradford, M. A.: Temperature and soil organic matter decomposition rates - synthesis of current knowledge and a way forward, Glob. Chang. Biol., 17(11), 3392–3404, 2011.

Cotrufo, M. F., Wallenstein, M. D., Boot, C. M., Denef, K. and Paul, E.: The Microbial Efficiency-Matrix Stabilization (MEMS) framework integrates plant litter decomposition with soil organic matter stabilization: do labile plant inputs form stable soil organic matter?, Glob. Chang. Biol., 19(4), 988–95, 2013.

Davidson, E. A. and Janssens, I. A.: Temperature sensitivity of soil carbon decomposition and feedbacks to climate change, Nature, 440, 165–173, 2006.

Dimassi, B., Cohan, J.-P., Labreuche, J. and Mary, B.: Changes in soil carbon and nitrogen following tillage conversion in a long-term experiment in Northern France, Agric. Ecosyst. Environ., 169, 12–20, 2013.

Dubbert, M., Mosena, A., Piayda, A., Cuntz, M., Correia, A. C., Pereira, J. S. and Werner, C.: Influence of tree cover on herbaceous layer development and carbon and water fluxes in a Portuguese cork-oak woodland, Acta Oecologica, 59, 35–45, 2014.

Dufour, L., Metay, A., Talbot, G. and Dupraz, C.: Assessing Light Competition for Cereal Production in Temperate Agroforestry Systems using Experimentation and Crop Modelling, J. Agron. Crop Sci., 199(3), 217–227, 2013.

Dunbabin, V. M., Postma, J. A., Schnepf, A., Pagès, L., Javaux, M., Wu, L., Leitner, D., Chen, Y. L., Rengel, Z. and Diggle, A. J.: Modelling root-soil interactions using three-dimensional models of root growth, architecture and function, Plant Soil, 372(1–2), 93–124, 2013.

Dupuy, L., Gregory, P. J. and Bengough, A. G.: Root growth models: Towards a new generation

959 of continuous approaches, J. Exp. Bot., 61(8), 2131–2143, 2010.

960 Duursma, R. and Medlyn, B.: MAESPA: a model to study interactions between water
961 limitation, environmental drivers and vegetation function at tree and stand levels, with an
962 example application to [CO_2] × drought interactions, Geosci. Model Dev., 5, 919–940, 2012.

963 Eilers, K. G., Debenport, S., Anderson, S. and Fierer, N.: Digging deeper to find unique
964 microbial communities: The strong effect of depth on the structure of bacterial and archaeal
965 communities in soil, Soil Biol. Biochem., 50, 58–65, 2012.

966 Eissenstat, D. M. and Yanai, R. D.: The Ecology of Root Lifespan, Adv. Ecol. Res., 27, 1–60,
967 1997.

968 Ellert, B. H. and Bettany, J. R.: Calculation of organic matter and nutrients stored in soils under
969 contrasting management regimes, Can. J. Soil Sci., 75, 529–538, 1995.

970 Elzein, A. and Balesdent, J.: Mechanistic simulation of vertical distribution of carbon
971 concentrations and residence times in soils, Soil Sci. Soc. Am. J., 59, 1328–1335, 1995.

972 Fierer, N., Schimel, J. P. and Holden, P. A.: Variations in microbial community composition
973 through two soil depth profiles, Soil Biol. Biochem., 35(1), 167–176, 2003.

974 Fontaine, S., Barot, S., Barré, P., Bdioui, N., Mary, B. and Rumpel, C.: Stability of organic
975 carbon in deep soil layers controlled by fresh carbon supply, Nature, 450, 277–281, 2007.

976 Germon, A., Cardinael, R., Prieto, I., Mao, Z., Kim, J. H., Stokes, A., Dupraz, C., Laclau, J.-P.
977 and Jourdan, C.: Unexpected phenology and lifespan of shallow and deep fine roots of walnut
978 trees grown in a silvoarable Mediterranean agroforestry system, Plant Soil, 401, 409–426, 2016.

979 Graves, A. R., Burgess, P. J., Palma, J. H. N., Herzog, F., Moreno, G., Bertomeu, M., Dupraz,
980 C., Liagre, F., Keesman, K., van der Werf, W., de Nooy, a. K. and van den Briel, J. P.:
981 Development and application of bio-economic modelling to compare silvoarable, arable, and
982 forestry systems in three European countries, Ecol. Eng., 29(4), 434–449, 2007.

983 Graves, A. R., Burgess, P. J., Palma, J., Keesman, K. J., van der Werf, W., Dupraz, C., van
984 Keulen, H., Herzog, F. and Mayus, M.: Implementation and calibration of the parameter-sparse
985 Yield-SAFE model to predict production and land equivalent ratio in mixed tree and crop
986 systems under two contrasting production situations in Europe, Ecol. Modell., 221, 1744–1756,
987 2010.

988 van Groenigen, K. J., Qi, X., Osenberg, C. W., Luo, Y. and Hungate, B. A.: Faster
989 decomposition under increased atmospheric CO_2 limits soil carbon storage, Science., 344, 508–
990 509, 2014.

991 Guenet, B., Eglin, T., Vasilyeva, N., Peylin, P., Ciais, P. and Chenu, C.: The relative importance
992 of decomposition and transport mechanisms in accounting for soil organic carbon profiles,
993 Biogeosciences, 10(4), 2379–2392, 2013.

994 Guenet, B., Moyano, F. E., Peylin, P., Ciais, P. and Janssens, I. A.: Towards a representation
995 of priming on soil carbon decomposition in the global land biosphere model ORCHIDEE
996 (version 1.9.5.2), Geosci. Model Dev., 9, 841–855, 2016.

997 Haile, S. G., Nair, V. D. and Nair, P. K. R.: Contribution of trees to carbon storage in soils of
998 silvopastoral systems in Florida, USA, Glob. Chang. Biol., 16, 427–438, 2010.

999 Hendrick, R. L. and Pregitzer, K. S.: Temporal and depth-related patterns of fine root dynamics
1000 in northern hardwood forests, J. Ecol., 84, 167–176, 1996.

1001 Howlett, D. S., Moreno, G., Mosquera Losada, M. R., Nair, P. K. R. and Nair, V. D.: Soil
1002 carbon storage as influenced by tree cover in the Dehesa cork oak silvopasture of central-
1003 western Spain, J. Environ. Monit., 13(7), 1897–904, 2011.

1004 Ilstedt, U., Bargués Tobella, A., Bazié, H. R., Bayala, J., Verbeeten, E., Nyberg, G., Sanou, J.,
1005 Benegas, L., Murdiyarso, D., Laudon, H., Sheil, D. and Malmer, A.: Intermediate tree cover
1006 can maximize groundwater recharge in the seasonally dry tropics, Sci. Rep., 6, 21930, 2016.

1007 IUSS Working Group WRB: World Reference Base for Soil Resources 2006, first update 2007.
1008 World Soil Resources Reports No. 103. FAO, Rome., 2007.

1009 Jobbagy, E. G. and Jackson, R. B.: The vertical distribution of soil organic carbon and its
1010 relation to climate and vegetation, Ecol. Appl., 10, 423–436, 2000.

1011 Joslin, J. D., Gaudinski, J. B., Torn, M. S., Riley, W. J. and Hanson, P. J.: Fine-root turnover
1012 patterns and their relationship to root diameter and soil depth in a ^{14}C-labeled hardwood forest,
1013 New Phytol., 172, 523–535, 2006.

1014 Kätterer, T., Bolinder, M. A., Andrén, O., Kirchmann, H. and Menichetti, L.: Roots contribute
1015 more to refractory soil organic matter than above-ground crop residues, as revealed by a long-
1016 term field experiment, Agric. Ecosyst. Environ., 141, 184–192, 2011.

1017 Keiluweit, M., Bougoure, J. J., Nico, P. S., Pett-Ridge, J., Weber, P. K. and Kleber, M.: Mineral
1018 protection of soil carbon counteracted by root exudates, Nat. Clim. Chang., 5, 588–595, 2015.

1019 Kim, D.-G., Kirschbaum, M. U. F. and Beedy, T. L.: Carbon sequestration and net emissions
1020 of CH_4 and N_2O under agroforestry: Synthesizing available data and suggestions for future
1021 studies, Agric. Ecosyst. Environ., 226, 65–78 , 2016.

1022 Koarashi, J., Hockaday, W. C., Masiello, C. A. and Trumbore, S. E.: Dynamics of decadally
1023 cycling carbon in subsurface soils, J. Geophys. Res., 117, 1–13, 2012.

1024 Koven, C. D., Riley, W. J., Subin, Z. M., Tang, J. Y., Torn, M. S., Collins, W. D., Bonan, G.
1025 B., Lawrence, D. M. and Swenson, S. C.: The effect of vertically resolved soil biogeochemistry
1026 and alternate soil C and N models on C dynamics of CLM4, Biogeosciences, 10(11), 7109–
1027 7131, 2013.

1028 Lange, M., Eisenhauer, N., Sierra, C. A., Bessler, H., Engels, C., Griffiths, R. I., Mellado-
1029 Vázquez, P. G., Malik, A. A., Roy, J., Scheu, S., Steinbeiss, S., Thomson, B. C., Trumbore, S.
1030 E. and Gleixner, G.: Plant diversity increases soil microbial activity and soil carbon storage,

1031 Nat. Commun., 6, 6707, 2015.

1032 Lavelle, P.: Faunal activities and soil processes: adaptative strategy that determine ecosystem
1033 function., 1997.

1034 Li, F., Meng, P., Fu, D. and Wang, B.: Light distribution, photosynthetic rate and yield in a
1035 Paulownia-wheat intercropping system in China, Agrofor. Syst., 74(2), 163–172, 2008.

1036 Lorenz, K. and Lal, R.: Soil organic carbon sequestration in agroforestry systems. A review,
1037 Agron. Sustain. Dev., 34, 443–454, 2014.

1038 Luedeling, E., Smethurst, P. J., Baudron, F., Bayala, J., Huth, N. I., van Noordwijk, M., Ong,
1039 C. K., Mulia, R., Lusiana, B., Muthuri, C. and Sinclair, F. L.: Field-scale modeling of tree-crop
1040 interactions: Challenges and development needs, Agric. Syst., 142, 51–69, 2016.

1041 Mead, R. and Willey, R. W.: The concept of a "land equivalent ratio" and advantages in yields
1042 from intercropping, Exp. Agric., 16(3), 217–228, 1980.

1043 Moreno, G., Obrador, J. J., Cubera, E. and Dupraz, C.: Fine root distribution in Dehesas of
1044 central-western Spain, Plant Soil, 277(1–2), 153–162, 2005.

1045 Moyano, F. E., Vasilyeva, N., Bouckaert, L., Cook, F., Craine, J., Curiel Yuste, J., Don, A.,
1046 Epron, D., Formanek, P., Franzluebbers, A., Ilstedt, U., Kätterer, T., Orchard, V., Reichstein,
1047 M., Rey, A., Ruamps, L., Subke, J. A., Thomsen, I. K. and Chenu, C.: The moisture response
1048 of soil heterotrophic respiration: Interaction with soil properties, Biogeosciences, 9, 1173–
1049 1182, 2012.

1050 Moyano, F. E., Manzoni, S. and Chenu, C.: Responses of soil heterotrophic respiration to
1051 moisture availability: An exploration of processes and models, Soil Biol. Biochem., 59, 72–85,
1052 2013.

1053 Mulia, R. and Dupraz, C.: Unusual fine root distributions of two deciduous tree species in
1054 southern France: What consequences for modelling of tree root dynamics?, Plant Soil, 281, 71–

85, 2006.

Mulia, R., Dupraz, C. and van Noordwijk, M.: Reconciling root plasticity and architectural ground rules in tree root growth models with voxel automata, Plant Soil, 337(1–2), 77–92, 2010.

Nair, P. K.: An introduction to agroforestry, Kluwer Academic Publishers, Dordrecht, The Netherlands., 1993.

Nair, P. K. R.: Classification of agroforestry systems, Agrofor. Syst., 3(2), 97–128, 1985.

van Noordwijk, M. and Lusiana, B.: WaNuLCAS, a model of water, nutrient and light capture in agroforestry systems, Agrofor. Syst., 43, 217–242, 1999.

Odhiambo, H. O., Ong, C. K., Deans, J. D., Wilson, J., Khan, A. A. H. and Sprent, J. I.: Roots, soil water and crop yield: Tree crop interactions in a semi-arid agroforestry system in Kenya, Plant Soil, 235(2), 221–233, 2001.

Oelbermann, M. and Voroney, R. P.: And evaluation of the century model to predict soil organic carbon: examples from Costa Rica and Canada, Agrofor. Syst., 82, 37–50, 2011.

Oelbermann, M., Voroney, R. P. and Gordon, A. M.: Carbon sequestration in tropical and temperate agroforestry systems: a review with examples from Costa Rica and southern Canada, Agric. Ecosyst. Environ., 104, 359–377, 2004.

Oelbermann, M., Voroney, R. P., Thevathasan, N. V., Gordon, A. M., Kass, D. C. L. and Schlönvoigt, A. M.: Soil carbon dynamics and residue stabilization in a Costa Rican and southern Canadian alley cropping system, Agrofor. Syst., 68(1), 27–36, 2006.

Ong, C. K. and Leakey, R. R. B.: Why tree-crop interactions in agroforestry appear at odds with tree-grass interactions in tropical savannahs, Agrofor. Syst., 45(1–3), 109–129, 1999.

Parton, W. J., Schimel, D. S., Cole, C. V and Ojima, D. S.: Analysis of factors controlling soil organic matter levels in great plains grasslands, Soil Sci. Soc. Am. J., 51, 1173–1179, 1987.

Peichl, M., Thevathasan, N. V, Gordon, A. M., Huss, J. and Abohassan, R. A.: Carbon sequestration potentials in temperate tree-based intercropping systems, southern Ontario, Canada, Agrofor. Syst., 66, 243–257, 2006.

Perveen, N., Barot, S., Alvarez, G., Klumpp, K., Martin, R., Rapaport, A., Herfurth, D., Louault, F. and Fontaine, S.: Priming effect and microbial diversity in ecosystem functioning and response to global change: A modeling approach using the SYMPHONY model, Glob. Chang. Biol., 20(4), 1174–1190, 2014.

Price, G. W. and Gordon, A. M.: Spatial and temporal distribution of earthworms in a temperate intercropping system in southern Ontario, Canada, Agrofor. Syst., 44, 141–149, 1999.

Prieto, I., Roumet, C., Cardinael, R., Kim, J., Maeght, J.-L., Mao, Z., Portillo, N., Thammahacksa, C., Dupraz, C., Jourdan, C., Pierret, A., Roupsard, O. and Stokes, A.: Root functional parameters along a land-use gradient: evidence of a community-level economics spectrum, J. Ecol., 103, 361–373, 2015.

Prieto, I., Stokes, A. and Roumet, C.: Root functional parameters predict fine root decomposability at the community level, J. Ecol., 104, 725–733, 2016.

R Development Core Team: R: A language and environment for statistical computing, 2013.

Rasse, D. P., Mulder, J., Moni, C. and Chenu, C.: Carbon turnover kinetics with depth in a French loamy soil, Soil Sci. Soc. Am. J., 70, 2097–2105, 2006.

Salomé, C., Nunan, N., Pouteau, V., Lerch, T. Z. and Chenu, C.: Carbon dynamics in topsoil and in subsoil may be controlled by different regulatory mechanisms, Glob. Chang. Biol., 16, 416–426, 2010.

Santaren, D., Peylin, P., Viovy, N. and Ciais, P.: Optimizing a process-based ecosystem model with eddy-covariance flux measurements: A pine forest in southern France, Global Biogeochem. Cycles, 21, 1–15, 2007.

Schwarz, G.: Estimating dimension of a model, Ann. Stat., 6(2), 461–464, 1978.

Shahzad, T., Chenu, C., Genet, P., Barot, S., Perveen, N., Mougin, C. and Fontaine, S.: Contribution of exudates, arbuscular mycorrhizal fungi and litter depositions to the rhizosphere priming effect induced by grassland species, Soil Biol. Biochem., 80, 146–155, 2015.

Sierra, C. A., Trumbore, S. E., Davidson, E. A., Vicca, S. and Janssens, I.: Sensitivity of decomposition rates of soil organic matter with respect to simultaneous changes in temperature and moisture, J. Adv. Model. Earth Syst., 7, 335–356, 2015.

Soetaert, K., Petzoldt, T. and Woodrow Setzer, R.: Solving Differential Equations in R: Package deSolve, J. Stat. Softw., 33(9), 1–25, 2010.

Somarriba, E.: Revisiting the past: an essay on agroforestry definition, Agrofor. Syst., 19(3), 233–240, 1992.

Steinbeiss, S., Beßler, H., Engels, C., Temperton, V. M., Buchmann, N., Roscher, C., Kreutziger, Y., Baade, J., Habekost, M. and Gleixner, G.: Plant diversity positively affects short-term soil carbon storage in experimental grasslands, Glob. Chang. Biol., 14(12), 2937–2949, 2008.

Sulman, B. N., Phillips, R. P., Oishi, A. C., Shevliakova, E. and Pacala, S. W.: Microbe-driven turnover offsets mineral-mediated storage of soil carbon under elevated CO_2, Nat. Clim. Chang., 4, 1099–1102, 2014.

Taghizadeh-Toosi, A., Christensen, B. T., Hutchings, N. J., Vejlin, J., Kätterer, T., Glendining, M. and Olesen, J. E.: C-TOOL: A simple model for simulating whole-profile carbon storage in temperate agricultural soils, Ecol. Modell., 292, 11–25, 2014.

Talbot, G.: L'intégration spatiale et temporelle du partage des ressources dans un système agroforestier noyers-céréales: une clef pour en comprendre la productivité ?, PhD Dissertation, Université Montpellier II., 2011.

Tarantola, A.: Inverse problem theory: methods for data fitting and model parameter estimation, edited by Elsevier., 1987.

Tarantola, A.: Inverse Problem Theory and Methods for Model Parameter Estimation, edited by SIAM., 2005.

Thevathasan, N. V. and Gordon, A. M.: Poplar leaf biomass distribution and nitrogen dynamics in a poplar-barley intercropped system in southern Ontario, Canada, Agrofor. Syst., 37, 79–90, 1997.

Udawatta, R. P., Kremer, R. J., Adamson, B. W. and Anderson, S. H.: Variations in soil aggregate stability and enzyme activities in a temperate agroforestry practice, Appl. Soil Ecol., 39(2), 153–160, 2008.

Virto, I., Barré, P., Burlot, A. and Chenu, C.: Carbon input differences as the main factor explaining the variability in soil organic C storage in no-tilled compared to inversion tilled agrosystems, Biogeochemistry, 108, 17–26, 2012.

van der Werf, W., Keesman, K., Burgess, P., Graves, A., Pilbeam, D., Incoll, L. D., Metselaar, K., Mayus, M., Stappers, R., van Keulen, H., Palma, J. and Dupraz, C.: Yield-SAFE: A parameter-sparse, process-based dynamic model for predicting resource capture, growth, and production in agroforestry systems, Ecol. Eng., 29(4), 419–433, 2007.

Wutzler, T. and Reichstein, M.: Colimitation of decomposition by substrate and decomposers - a comparison of model formulations, Biogeosciences, 5, 749–759, 2008.

Wutzler, T. and Reichstein, M.: Priming and substrate quality interactions in soil organic matter models, Biogeosciences, 10(3), 2089–2103, 2013.

Yin, R. and He, Q.: The spatial and temporal effects of paulownia intercropping: The case of northern China, Agrofor. Syst., 37, 91–109, 1997.

Zhang, W., Wang, X. and Wang, S.: Addition of external organic carbon and native soil organic

carbon decomposition: a meta-analysis., PLoS One, 8(2), e54779, 2013.